Control Engineering Practice 165 (2025) 106514

Contents lists available at ScienceDirect

Control Engineering Practice

journal homepage: www.elsevier.com/locate/conengprac

Offset-free stochastic quadratic dynamic matrix control formulations using polynomial chaos expansions☆

Wallace Gian Yion Tan [a], Krystian Ganko [a], Srimanta Santra [a], Matthias von Andrian [b], Richard D. Braatz [a,*]

[a] Massachusetts Institute of Technology, 77 Massachusetts Avenue, Cambridge, MA 02139, USA
[b] Whirlpool Corporation, 2000 N. M-63, Benton Harbor, MI 49022, USA

ARTICLE INFO

Keywords:
Polynomial chaos theory
Stochastic model predictive control
Quadratic dynamic matrix control
Closed-loop stability analysis

ABSTRACT

Probabilistic uncertainties in the model parameters result in distributional uncertainties in the model predictions. While such uncertainty descriptions have been incorporated into model predictive control (MPC) formulations using polynomial chaos theory (PCT), more care is required to ensure integral action than in traditional MPC. This article thoroughly examines offset-free formulations of PCT-based MPC for multiple-input, multiple-output linear time-invariant systems. We compile, prove, and validate features of multiple stochastic MPC formulations. Under mild assumptions, these features include (i) guarantees for the existence of a full column-rank integrator to eliminate offset in multiple performance indices; (ii) guarantees of nominal closed-loop stability for the unconstrained systems, and (iii) computationally efficient, spectrally accurate resolution of parametric uncertainty. Application of our stochastic MPC formulations to setpoint tracking and disturbance rejection in numerical case studies demonstrate the asymptotic removal of offset in *all* higher-order contributions to output variation due to parametric uncertainty.

1. Introduction

Stochastic Model Predictive Control (SMPC) is a form of Model Predictive Control (MPC) that explicitly accounts for stochastic noise, disturbances, and parametric uncertainties (Heirung, Paulson, O'Leary, & Mesbah, 2018; Morari & Lee, 1999). SMPC accounts for the stochastic nature of state trajectories by optimizing a specific loss function over the entire probability distribution of state trajectories (Mesbah, 2016). Manipulated variable constraints are deterministic whereas state and output constraints in SMPC can be specified in expectations on certain variables or as chance constraints which restrict the probability of specified events. SMPC has been proposed for applications where handling uncertainty is critical such as in quantitative finance (Bemporad, Puglia, & Gabbriellini, 2011), autonomous vehicle path planning (Mammarella et al., 2018), and control of manufacturing processes (Heirung et al., 2018; Tian, Prakash, Zavala, Olson, & Gopaluni, 2020; Van Hessem & Bosgra, 2006).

SMPC is computationally more expensive than MPC, as the space of feasible state trajectories to numerically optimize over is significantly enlarged by process stochasticity. As such, a fundamental challenge of SMPC is the formulation of an on-line, low computational cost method able to effectively propagate uncertainty forward and preserve information on the probability distribution of the outputs (Mesbah, 2016). This need motivates the use of Polynomial Chaos Theory (PCT) in SMPC, which is a method of expressing a random variable in terms of a sum of orthogonal polynomials of another random variable (e.g., Hermite Polynomials of Gaussian Variables Cameron & Martin, 1947). While the control based on a process model with probabilistic parameter uncertainties is inherently harder than control based on a comparable nominal model, PCE provides a systematic way of approximating the stochastic system to any degree of accuracy. Early work applied this method of approximation to uncertain systems modeled by random ordinary differential equations (ODEs) (Xiu & Karniadakis, 2002),[1] with later extensions to partial differential equations with uncertain

☆ This manuscript is an extension of von Andrian and Braatz (2019).

* Corresponding author.
E-mail address: braatz@mit.edu (R.D. Braatz).

[1] Although Xiu and Karniadakis (2002) discusses PCT applied to stochastic differential equations (SDEs), a more appropriate terminology would be PCE applied to random ODEs. Put simply: for SDEs, due to additional randomness imparted by an additive white noise term, the output random variable trajectories are not uniquely determined when the uncertain parameter vector θ is known *a priori*. However, for random ODEs, if θ is known, then the output random variable trajectories are uniquely determined. The interested reader may find (Filip, Javeed, & Trefethen, 2019) and references therein useful.

https://doi.org/10.1016/j.conengprac.2025.106514
Received 9 March 2025; Received in revised form 8 June 2025; Accepted 23 July 2025
Available online 14 August 2025

parameters (Lucia, Zometa, Kögel, & Findeisen, 2015; Luo, 2006). In numerous case studies, PCT has been shown to reduce the computational costs of trajectory optimization while simultaneously performing highly accurate uncertainty propagation (Kim & Braatz, 2012; Lucia et al., 2015; Lucor, Su, & Karniadakis, 2004; Paulson, Streif, Findeisen, Braatz, & Mesbah, 2018). Recently, PCT has been incorporated into optimal and robust control algorithms to systematically address parametric uncertainties and estimate probabilities of rare events (Hsu & Bhattacharya, 2020; Piprek, Gros, & Holzapfel, 2019a, 2019b).

The use of PCT-based SMPC in manufacturing processes with high-dimensional output spaces was demonstrated by Paulson, Mesbah, Streif, Findeisen, and Braatz (2014). Although the approach significantly reduced the effects of uncertainty on the controlled variables, the formulations were not designed to be offset-free. That is, the process outputs did not necessarily converge asymptotically in time to new setpoints for step changes in the setpoints. Offset-free control is a desirable property in many applications (Maeder, Borrelli, & Morari, 2009; Maeder & Morari, 2010; Muske & Badgwell, 2002), because the setpoint usually represents a current optimal operating point of the process, such as the current demand or composition of a product (Luyben, 2007). Such applications motivate the formulation of a provably offset-free SMPC control strategy.

Motivated by the above considerations, this work describes a suite of offset-free formulations of SMPC that integrate PCT into Quadratic Dynamic Matrix Control (QDMC). QDMC is a control algorithm that is widely used in industry, due to its good setpoint tracking properties and its ability to handle input and output constraints and multiple-input, multiple-output (MIMO) systems (Garcia & Morshedi, 1986). The optimization in QDMC can be formulated as a quadratic program (QP), which can be solved efficiently by convex optimization solvers (Morari & Lee, 1999). Galerkin projection of the stochastic model is used to obtain a deterministic model of PC coefficients, which is then fed to QDMC-based SMPC formulations (Garcia & Morshedi, 1986). We present SMPC formulations that guarantee zero offset and nominal closed-loop stability of the unconstrained systems. In particular, we prove our SMPC formulations to contain a full-column rank integrator with the appropriate choice of controller variables and weights, which leads to zero offset and closed-loop stability.

Regarding the novelty of this work, we emphasize that previous provably offset-free QDMC formulations for MIMO systems produce zero offset by including additive integrating disturbance terms in *parametrically certain* models (see, e.g., Morari and Lee (1999) and Pannocchia and Rawlings (2003) and references therein). These results, furthermore, are foundational and span decades of literature from the 1970s to the early 2000s. The present work demonstrates provably offset-free QDMC formulations for *parametrically uncertain* models, where, in addition to additive integrating disturbance terms, we must consider disturbance terms arising from multiplicative parametric uncertainty in the modeled dynamics (Morari & Zafiriou, 1989). More specifically, our approach using PCT distinguishes from existing scenario-based or constraint-tightening and stochastic tube-based methods which synthesize controllers for similar systems (see, e.g., Arcari, Iannelli, Carron, and Zeilinger (2023) and Fagiano, Schildbach, Tanaskovic, and Morari (2015) and references therein). The development of our formulations necessarily depends on theorems and lemmas in previous work. In order to both preserve continuity in and contribute novelty to the existing discussion, we delineate our key results from previous theorems and lemmas with references to Appendix.

The article is organized as follows. Section 2 provides mathematical background on linear time-invariant (LTI) systems, step-response models, QDMC, and MIMO closed-loop integral action. Section 3 presents a proof that (unconstrained) QDMC controller formulation in MIMO LTI systems contains a full column-rank integrator under mild conditions on the plant LTI system coefficients and controller weights. Section 4 describes PCT and Galerkin projection for LTI systems in SMPC. Section 5 describes our main contributions to PCT-based QDMC formulations that guarantee nominal and robust stability. Finally, Sections 6 and 7 provide two illustrative numerical case studies. The first case is the control of a small-scale series–parallel reaction network in a continuously stirred tank reactor (CSTR). The second case is the control of a large-scale network of heat exchangers. Both cases demonstrate the effectiveness of PCT-based QDMC formulations in achieving accurate forward uncertainty propagation and offset-free control with robust closed-loop performance.

This article significantly expands on a conference paper (von Andrian & Braatz, 2019) by extending the methodology to the MIMO case, providing precise statements of the theoretical results, providing proofs of all the theoretical results, discussing additional formulations for nominal and robust stability, and validating the methodology on two more challenging case studies, with one having a high-dimensional state space.

2. Definitions and preliminary background

This section defines the class of MIMO LTI process models studied in this article. For context, first we briefly describe the formulation of *deterministic* QDMC in terms of the step-response matrices of the process models (see, e.g., Qin and Badgwell (2003) and references therein). Then a series of lemmas are given that rigorously define conditions for (i) open- and closed-loop system bounded-input, bounded-output (BIBO) stability, (ii) additive disturbance-free closed-loop integral action in the MIMO system, and (iii) offset-free control in the multiple performance index case due to having a full column-rank integrator in the controller. We finally use these definitions to prove that unconstrained QDMC for the MIMO case is offset-free in multiple performance indices.

2.1. Definitions and notations

Denote $\mathbb{N} = \{0, 1, 2, \dots\}$ as the natural numbers, 1^p as the vector of ones of dimension p, $0_n, I_n \in \mathbb{R}^{n\times n}$ as the zero and identity matrices respectively, and $\mathbb{1}_\Omega$ as the indicator function on the set $\Omega \in \mathbb{R}^n$. For $x \in \mathbb{R}^n$, denote $\|x\|$ as the Euclidean norm of x. Given square matrices $W_i \in \mathbb{R}^{n_i\times n_i}$ and column vectors $v_i \in \mathbb{R}^{n_i}$ where $i = 1, 2, \dots, k$ and n_i are non-zero positive integers, denote the block-diagonal matrix construction as

$$\operatorname{diag}[W_1, W_2, \dots, W_k] = \begin{bmatrix} W_1 & & \\ & \ddots & \\ & & W_k \end{bmatrix} \in \mathbb{R}^{(\sum_i n_i)\times(\sum_i n_i)},$$

and the column-vector concatenation as

$$\operatorname{vec}[v_1, v_2, \dots, v_k] = \begin{bmatrix} v_1 \\ \vdots \\ v_k \end{bmatrix} \in \mathbb{R}^{\sum_i n_i}.$$

Given matrices $A \in \mathbb{R}^{a\times b}$ and $B \in \mathbb{R}^{c\times d}$, denote $A \otimes B \in \mathbb{R}^{(ac)\times(bd)}$ as the Kronecker product of A and B (Brewer, 1978). Denote $\|\cdot\|_2$ and $\|\cdot\|_F$ as the spectral and Frobenius norms of A, respectively. All deviations from these notations will be noted explicitly at the time of use.

2.2. Linear time-invariant systems and step-response models

Consider the impulse response of a discrete-time MIMO LTI system,

$$y(t) := \sum_{i=1}^{\infty} H_i u(t-i), \tag{1}$$

where $t \in \mathbb{N}$ is the time index, $y \in \mathbb{R}^{n_y}$ is the output vector, $u \in \mathbb{R}^{n_u}$ is the input vector, and $H_i \in \mathbb{R}^{n_y\times n_u}$ are unit-impulse response matrices. Assume that $u(t) = 0$ for $t \le 0$, which implies that $y(0) = 0$, i.e., the system is operating at steady state at the initial time. The formulation (1) implicitly assumes that $H_0 = 0$, implying that the current output only depends on previous inputs so as not to violate causality. For any system (1) that is BIBO stable, the coefficients H_i are absolutely summable,

i.e., $\sum_i \|H_i\| < \infty$. Restrict the system (1) to have finite memory of the past, that is, $H_i = 0$ for $i > N$ where $N \in \mathbb{N}$ is defined as the truncation number. The value of N is selected based on the system dynamics and sampling time used for system identification, e.g., industrial implementations typically choose sampling time so that $N = 30$ is large enough to capture the system dynamics (Cutler & Ramaker, 1980). When N is poorly chosen, truncation errors due to model-plant mismatch accumulate and performance of the predictive model becomes poor (Lundström, Lee, Morari, & Skogestad, 1995). These assumptions are all very reasonable for industrial application, for which MPC is applied on top of pre-stabilized lower level regulatory loops, e.g., see Morari and Lee (1999) and Qin and Badgwell (2003) and references therein.

After introducing control input differences $\Delta u(t) := u(t) - u(t-1)$, the impulse-response model (1) can be reformulated as

$$y(t) = \sum_{i=1}^{\infty} G_i \Delta u(t-i), \tag{2}$$

where $G_i := \sum_{j=i}^{\infty} H_j$ are the unit step-response coefficient matrices. Since $H_i = 0$ for $i > N$, it follows that $G_i = G_N$ for $i > N$. The summation in (2) has finitely many terms) because $\Delta u(t-i) = 0$ for all $i \geq t$. The step-response coefficient matrices G_i can be calculated by applying a unit step input to the system for each input variable, either from data or from any model of the process. The truncation time N is chosen as the value at which the step-response coefficient matrices G_i asymptotically approach some constant value for unit step inputs (Finn, Wahlberg, & Ydstie, 1993).

Dynamic matrix control (DMC) is an MPC algorithm that uses the unit step-response model (2) to predict the system output within the prediction horizon. The model is fed to an on-line optimization to compute the current and future time control actions, i.e., $u(t)^*, u(t+1)^*, \ldots$, which optimize the performance objectives over a prediction horizon.

Suppose that, for a real process, either a process simulator or system identification procedures (see, e.g., Ljung (1999) and references therein) indicate the validity of a dynamic input–output response structure of the form (2). Denoting $p \in \mathbb{N}$ as the finite length of the prediction horizon, the model (1) is constructed for each current time t and provides predictions $\hat{y}(t+k|t)$ of the real process outputs $y(t+k|t)$ at future times $t+k$ where $k \in \{1, 2, \ldots, p\}$. In other words, a total of pn_y scalar outputs are computed at each time step by an imperfect process model which is conditioned on information from all prior times. Encoding these details, DMC uses the predictive model formulation

$$\hat{y}(t+k|t) := \sum_{i=1}^{\infty} G_i \Delta u(t+k-i) + \hat{n}(t+k|t), \tag{3}$$

where $\hat{n}(t+k|t)$ is a modeled disturbance term to account for model-plant mismatch at the current time. DMC estimates the process disturbance as the current difference between the true output response and measured output response, i.e., $\hat{n}(t+k|t) := y_{\mathrm{m}}(t) - y(t), k \geq 0$. For further analysis, the key contributions to the system response under (3) can be distinguished by rearranging the terms as

$$\begin{aligned}
\hat{y}(t+k|t) &= \sum_{i=1}^{\infty} G_i \Delta u(t+k-i) + \hat{n}(t+k|t) && \text{(4a)}\\
&= \sum_{i=1}^{k} G_i \Delta u(t+k-i) \\
&\quad + \sum_{i=k+1}^{\infty} G_i \Delta u(t+k-i) + \hat{n}(t+k|t) && \text{(4b)}\\
&= \sum_{i=1}^{k} G_i \Delta u(t+k-i) + f(t+k|t) + \hat{n}(t+k|t), && \text{(4c)}
\end{aligned}$$

where

$$f(t+k|t) := \sum_{i=k+1}^{\infty} G_i \Delta u(t+k-i) \tag{5}$$

is the free response at time $t+k$ during the iteration at time t. For the current time (i.e., when $k = 0$), the above assumptions and constructions imply that $f(t|t) = y(t)$, which further implies that $\hat{n}(t+k|t) = y_{\mathrm{m}}(t) - f(t|t)$. Intuitively, the first term in (4c) represents the forced response, which is the system output response due to the changes in the control inputs in the future. The second term is the free response, which is the system output response when there are no step changes in the control inputs in the future (i.e., $\Delta u(t+k) = 0$ for all $k \geq 0$, that is, $u(t+k) = u(t-1)$ for all $k \geq 0$). The last term is the measured disturbance at the current time.

2.3. Quadratic dynamic matrix control

QDMC is the form of DMC that uses a quadratic objective function to quantify process and controller performance, e.g., rapid setpoint tracking and disturbance rejection with constraints on actuation (Garcia & Morshedi, 1986). At each process time t, QDMC is given the current measurement $y_{\mathrm{m}}(t)$ and a desired setpoint $y_{\mathrm{sp}}(t)$ to compute the current and future time optimal input step changes $\Delta u(t)^*, \Delta u(t+1)^*, \ldots$ subject to process and control input constraints. The optimal inputs are obtained by solving a constrained QP, that is, an optimization that minimizes a quadratic function over a polytopic constraint set on the inputs and outputs (Nocedal & Wright, 2006).

More specifically, QDMC uses the process model in (4c)–(5) to predict the future p outputs in the prediction horizon and to minimize a quadratic objective function $\mathcal{J} \in \mathbb{R}_{\geq 0}$ over the next $c \in \mathbb{N}$ control action step changes $\Delta u(t), \Delta u(t+1), \ldots, \Delta u(t+c-1)$, where $c \leq p$ is termed the control horizon. Defining

$$e(t+i|t) := \hat{y}(t+i|t) - y_{\mathrm{sp}}(t+i) \tag{6}$$

as the predicted setpoint error (aka offset from setpoint), the optimal control objective is

$$\mathcal{J} := \sum_{i=1}^{p} e(t+i|t)^{\top} W_{yi} e(t+i|t) + \sum_{i=1}^{c} \Delta u(t+i-1)^{\top} W_{ui} \Delta u(t+i-1), \tag{7}$$

where all weight matrices $W_{yi} \in \mathbb{R}^{n_y \times n_y}$ and $W_{ui} \in \mathbb{R}^{n_u \times n_u}$ are designed to be positive definite. The weight matrices encode the trade-off between setpoint tracking and actuation magnitude. Introducing output path constraints and control input limitations, the convex QP solved by QDMC becomes

$$\begin{aligned}
\min_{\mathcal{U}} \quad & \mathcal{J} \\
\text{s.t.} \quad & A_i \hat{y}(t+i|t) \leq b_i, \quad \forall i \in \{1, 2, \ldots, p\}, \\
& u_{\min} \leq u(t+i-1) \leq u_{\max}, \quad \forall i \in \{1, 2, \ldots, c\}, \\
& \Delta u_{\min} \leq \Delta u(t+i-1) \leq \Delta u_{\max}, \quad \forall i \in \{1, 2, \ldots, c\},
\end{aligned} \tag{8}$$

where $\mathcal{U} := \{\Delta u(t), \Delta u(t+1), \ldots, \Delta u(t+c-1)\}$, and $A_i \in \mathbb{R}^{m \times n_y}$, $b_i \in \mathbb{R}^m$, and $u_{\min}$, $u_{\max}$, $\Delta u_{\min}$, $\Delta u_{\max} \in \mathbb{R}^{n_u}$ specify the constraints. To simplify notation, denote

$$\Delta \mathbf{u}(t) := \mathrm{vec}[\Delta u(t), \Delta u(t+1), \ldots, \Delta u(t+c-1)], \tag{9a}$$

$$\hat{\mathbf{y}}(t) := \mathrm{vec}[\hat{y}(t+1|t), \hat{y}(t+2|t), \ldots, \hat{y}(t+p|t)], \tag{9b}$$

$$\mathbf{y}_{\mathrm{sp}}(t) := \mathrm{vec}[y_{\mathrm{sp}}(t+1), y_{\mathrm{sp}}(t+2), \ldots, y_{\mathrm{sp}}(t+p)], \tag{9c}$$

$$\mathbf{e}(t) := \hat{\mathbf{y}}(t) - \mathbf{y}_{\mathrm{sp}}(t), \tag{9d}$$

$$W_y := \mathrm{diag}[W_{y1}, W_{y2}, \ldots, W_{yp}], \tag{9e}$$

$$W_u := \mathrm{diag}[W_{u1}, W_{u2}, \ldots, W_{uc}], \tag{9f}$$

where the predicted error signal $\mathbf{e}(t)$ depends on the previous control actions applied to the system. The convex quadratic structure of the objective function is seen in the expression

$$\mathcal{J}(\mathbf{e}(t), \Delta \mathbf{u}(t)) = \mathbf{e}(t)^{\top} W_y \mathbf{e}(t) + \Delta \mathbf{u}(t)^{\top} W_u \Delta \mathbf{u}(t). \tag{9g}$$

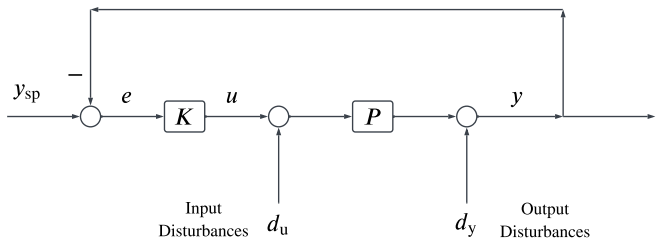

Fig. 1. Block diagram for the closed-loop system with additive disturbances d_u and d_y, and feedback structure with controller K.

For proving integral action and evaluating closed-loop performance in the sections that follow, the user-specified setpoint, which is an exogenous input to the system, is taken as constant. That is, $y_{sp}(t) = y_{sp}$ for all time t, which further implies that $\mathbf{y}_{sp}(t) = 1^p \otimes y_{sp}$. In both constrained and unconstrained QDMC, solving the convex QP in (8) at each sampling time t produces the optimal input step change series $\Delta\mathbf{u}(t)^*$. In practice, however, only the first optimal step change input $\Delta u(t)^*$ is actually applied to the system. The remaining $\Delta u(t+1)^*, \Delta u(t+2)^*, \ldots, \Delta u(t+c-1)^*$ solutions can be used to warm-start an initial guess to the QP solver at the next time step $t+1$. Therefore, the inputs $u(t)$ evolve via the control law

$$u(t) = u(t-1) + [I_{n_u} \; 0_{n_u} \; \cdots \; 0_{n_u}]\Delta\mathbf{u}(t)^*. \tag{10}$$

2.4. Multiple performance index offset-free control, Z-transforms, and transfer functions

Consider the closed-loop plant construction with multiple endogenous and exogenous inputs and outputs in Fig. 1. In defining the performance objectives and conditions for optimal controller synthesis (e.g., disturbance rejection, setpoint tracking), we pose the performance index vector, aka error vector, as $e(t) \in \mathbb{R}^{n_y}$. An integrator in the controller applied to an asymptotically stable single-input single-output system implies that — in the absence of measurement noise and disturbances — the error $e(t)$ asymptotically converges to zero when the specified setpoint y_{sp} is held constant (Rawlings, Mayne, & Diehl, 2017).[2] In other words, the formulation is offset-free in some single performance index. However, for a closed-loop MIMO response model, an integrator may or may not exist for every performance index, motivating controller designs with full column-rank integrators. These concepts and others are rigorously presented below.

The discrete-time transfer function from inputs to outputs are written in terms of the Z-transform.

Definition 1. [Z-transform, see, e.g., Chen (1984)] Let j denote the imaginary unit, $t \in \mathbb{N}$, and $z \in \mathbb{C}$. Given a sequence of vectors $x(t) \in \mathbb{R}^n$, the unilateral Z-transform of $x(t)$ is denoted as $X(z) \in \mathbb{C}^n$ and is given by

$$X(z) := \mathcal{Z}(x(t))(z) := \sum_{i=0}^{\infty} x(i) z^{-i}. \tag{11}$$

For a region $C \subset \mathbb{C}$ which encloses all points z for which summation (11) converges, the inverse Z-transform is defined by the contour integral

$$x(t) := \mathcal{Z}^{-1}(X(z))(t) := \frac{1}{2\pi j} \oint_C X(z) z^{t-1} \, \mathrm{d}z. \tag{12}$$

[2] This statement of integrator action also implies zero offset in the presence of any combination of constant values for the disturbance and setpoint, provided that the measurement noise n is zero.

Here we provide several pertinent MIMO LTI system lemmas. Although the lemmas are well-known in the control theory literature, the proofs are written out for completeness in the Appendix, with suggested references for further reading. Using these lemmas, we show that closed-loop integral action leads to offset-free control in MIMO LTI systems under mild conditions on the integrator matrix K_I. The transfer functions $G(z) \in \mathbb{R}^{m \times n}$ are assumed to only contain rational entries. A pole of the transfer function $G(z)$ is defined as a pole of any of the entries of $G(z)$. In general, for a linear system to be BIBO stable, its transfer function can only have poles strictly within the open unit circle, so that the impulse response coefficients remain absolutely summable. This is shown in the following lemma:

Lemma 1 (*BIBO Stability*)**.** *Suppose that $u(t) \in \mathbb{R}^n$ is a bounded input sequence. Let $y(t) \in \mathbb{R}^m$ denote the sequence of outputs, and suppose that $Y(z) = G(z)U(z)$ and all poles z_i of $G(z)$ lie within the open unit circle. Then the sequence $y(t)$ is bounded and $g(t)$ (the inverse Z-transform of $G(z)$) satisfies $\|g(t)\|_2 \le C_g\left((\max_i |z_i| + \epsilon)^t\right)$ for every $\epsilon > 0$ and some scalar, real-valued $C_g > 0$ which depends on ϵ.*

The proof of Lemma 1 is in Appendix A.1. The next lemma discusses intuition behind the presence of an integrator in the closed-loop of an LTI MIMO system response.

Lemma 2 (*Integrator Action*)**.** *Suppose that $U(z) = K(z)E(z)$ and the controller transfer function $K(z)$ is a matrix with rational entries, and $K(z) = K_I(z-1)^{-1} + \tilde{K}$, where $\tilde{K}$ has entries with poles all lying within the open unit circle. Then $u(t) = K_I \sum_{i=1}^{t} e(i) + d(t)$, where $d(t)$ is a bounded sequence.*

The proof of Lemma 2 is in Appendix A.2.

Remark 1. The matrix K_I is known as the *integrator* of the controller transfer function $K(z)$. Intuitively, for closed-loop systems, the integrator adds the errors $e(t)$ and multiplies by the matrix K_I. In the SISO case, K_I is a scalar, so as long as $K_I \neq 0$, the cumulative effect of the control action is always present. However, in the MIMO case, K_I may not be full column rank, so the cumulative effect of the errors may not be present in all output directions.

The next lemma is necessary to show that MIMO closed-loop integrator action is offset-free under some mild assumptions on the closed-loop transfer function.

Lemma 3 (*Multiple Performance Index Closed-Loop Integrator Action is Offset-free*)**.** *Suppose that $E(z) = G(z)Y_{sp}(z)$ and $G(z) = (z-1)^k \tilde{G}(z)$ for some integer $k \ge 1$, and $\tilde{G}(z)$ has no poles at $z = 1$. If all poles of $G(z)$ lie within the open unit circle and $\lim_{t\to\infty} y_{sp}(t) = c$, then the multiple performance index error vector $e(t) \in \mathbb{R}^{n_y}$ has the property $\lim_{t\to\infty} e(t) = 0$.*

The proof of Lemma 3 is in Appendix A.3. The main application of Lemmas 1–3 is to prove that certain formulations of controllers are offset-free, i.e., $\lim_{t\to\infty} y(t) = y_{sp}$. Consider the standard closed-loop feedback system in Fig. 1, with output disturbances d_y and input disturbances d_u. The transfer function of the MIMO LTI system is

$$P(z) = \sum_{i=1}^{N} H_i z^{-i}, \tag{13}$$

where the H_i are the impulse response coefficients in (1), so $P(z)$ is the Z-transform of the LTI system. Let $K(z)$ represent the transfer function of the controller. If the setpoint y_{sp} converges as in Lemma 3, assuming that $\left(I_{n_y} + P(z)K(z)\right)^{-1}$ exists and is proper,[3] the closed-loop exogenous-input, exogenous-output response using Z-transforms is

$$Y(z) = \left(I_{n_y} + P(z)K(z)\right)^{-1}\left(P(z)K(z)Y_{sp}(z) + D_y(z) + P(z)D_u(z)\right).$$

[3] This statement is equivalent to $I_{n_y} + P(\infty)K(\infty)$ being invertible (see, e.g., Lemma 5.1 of Zhou and Doyle (1998)).

where the setpoint $y_{sp} \in \mathbb{R}^{n_y}$, input disturbances $d_u \in \mathbb{R}^{n_u}$, and output disturbances $d_y \in \mathbb{R}^{n_y}$ are exogenous inputs into the system. Then the overall error response is

$$\begin{aligned} E(z) &= Y(z) - Y_{sp}(z) \\ &= \left(I_{n_y} + P(z)K(z)\right)^{-1}\left(-Y_{sp}(z) + D_y(z) + P(z)D_u(z)\right) \\ &= G_{sp}(z)Y_{sp}(z) + G_{d_y}(z)D_y(z) + G_{d_u}(z)D_u(z), \end{aligned}$$

which separates the transfer function contributions to the offset error resulting from $G_{sp}(z) = -G_{d_y}(z) = -\left(I_{n_y} + P(z)K(z)\right)^{-1}$ and $G_{d_u}(z) = \left(I_{n_y}+P(z)K(z)\right)^{-1}P(z)$. If the controller formulation $K(z)$ has an integrator then, under some mild conditions which follow from using Lemma 3, the formulation is offset-free. Specifically, assume that the transfer matrix for the plant $P(z)$ is BIBO stable, and assume that

$$K(z) = \frac{1}{z-1}K_I + \tilde{K}(z), \tag{14}$$

where $\tilde{K}(z)$ has no poles at $z = 1$. Note that $P(1) = G_N$, which is the steady-state response of the LTI in (1). In order to prevent pole-zero cancellation, we assume that $P(1)K_I$ is a full column-rank matrix. Intuitively, this means that the integrator K_I is sensitive to all directions of inputs which can induce change in the output from the plant $P(z)$. Note that

$$\lim_{z\to 1}(z-1)(I_{n_y} + P(z)K(z)) = P(1)K_I, \tag{15}$$

which, by inverting the equation above, further implies that

$$\lim_{z\to 1}\frac{1}{z-1}(I_{n_y} + P(z)K(z))^{-1} = (P(1)K_I)^{-1}, \tag{16}$$

and

$$\lim_{z\to 1}(I_{n_y} + P(z)K(z))^{-1} = \lim_{z\to 1}(z-1)(P(1)K_I)^{-1} = 0. \tag{17}$$

Therefore, $G_{sp}(z) = -(I_{n_y} + P(z)K(z))^{-1} = (z-1)\tilde{G}(z)$ where $\tilde{G}(z)$ has no poles at $z = 1$. By Lemma 3, checking that a controller is offset-free in multiple performance indices while in the presence of integrators reduces to inspecting whether (i) $G_{sp}(z)$ has poles within the open unit circle only and (ii) the disturbances d_y and d_u asymptotically converge to some constants as $t \to \infty$. A similar argument holds for the transfer function $G_{d_u}(z)$. The above discussions lead to Theorem 1.

Theorem 1. *Consider the closed-loop system with disturbances d_y and d_u in Fig. 1. Assume that the controller formulation $K(z)$ contains an integrator K_I, $P(1)K_I$ in (14) is full column rank (and thus invertible), and all poles of $G_{d_y} = -G_{sp} = (I_{n_y} + P(z)K(z))^{-1}$ and $G_{d_u}(z) = (I_{n_y} + P(z)K(z))^{-1}P(z)$ lie within the open unit circle. Then, the closed-loop system is offset-free in all n_y performance indices, i.e., $\lim_{t\to\infty} e(t) = 0$, if the limits $\lim_{t\to\infty} d_y$ and $\lim_{t\to\infty} d_u$ exist.*

In particular, when there are no plant input and output disturbances, i.e., $d_y = d_u = 0$, the controller formulation is offset-free when $K(z)$ has an integrator and no pole-zero cancellation occurs. In Sections 3 and 5, Theorem 1 is used to formulate offset-free controllers for unconstrained QDMC and PCE-based QDMC, respectively.

Remark 2. Theorem 1 shows that, if $P(1)$ is full column rank (which implies that the plant is controllable), a sufficient condition for closed-loop stability is that K_I has full column rank. Otherwise, the conclusion of Theorem 1 may not hold.

Theorem 1 formalizes a well-known fact that QDMC achieves offset-free regulation when appropriate weights are used (see, e.g., Morari and Lee (1999) and Qin and Badgwell (2003); technicalities follow in Section 3). Since this property is only tacitly assumed in the literature, we feel the need to distinguish Theorem 1 because the theorem implications demonstrate a fundamental strength of the PCE-based QDMC method (discussion follows in Section 5).

3. Offset-free unconstrained deterministic QDMC formulations

This section shows that unconstrained deterministic QDMC formulations contain a full column-rank integrator, which by Theorem 1 implies that the closed-loop system is offset-free in all performance indices. Following the discussion in Section 2.3, the input and output constraints are removed from (8) and, at every time t, the unconstrained convex QP

$$\min_{\Delta\mathbf{u}(t)} \mathcal{J}(\mathbf{e}(t), \Delta\mathbf{u}(t)), \tag{18}$$

is solved, where $\mathcal{J}(\mathbf{e}(t), \Delta\mathbf{u}(t))$ is given by (9g), and $\mathbf{e}(t)$, which is defined by (6) and (9d), depends linearly on future control actions $\Delta\mathbf{u}(t)$ as in (9a). Convex, unconstrained QPs have closed-form analytical solutions. First compute the gradient of (9g) with respect to $\Delta\mathbf{u}(t)$ by direct differentiation:

$$\begin{aligned} \frac{\partial\mathcal{J}}{\partial\Delta\mathbf{u}} &= 2\Delta\mathbf{u}(t)^\top W_u + 2\mathbf{e}(t)^\top W_y\frac{\partial\mathbf{e}}{\partial\Delta\mathbf{u}} \\ &= 2\Delta\mathbf{u}(t)^\top W_u + 2\mathbf{e}(t)^\top W_y\frac{\partial\hat{\mathbf{y}}}{\partial\Delta\mathbf{u}} \in \mathbb{R}^{1\times n_u c}, \end{aligned} \tag{19}$$

where the second equality holds by assuming y_{sp} does not depend on $\Delta\mathbf{u}(t)$. To compute the partial derivative of the MIMO LTI model predictions $\hat{\mathbf{y}}(t)$, expand (4c) into

$$\begin{aligned} \hat{\mathbf{y}}(t) &= \begin{bmatrix} \hat{y}(t+1|t) \\ \hat{y}(t+2|t) \\ \vdots \\ \hat{y}(t+p|t) \end{bmatrix} \\ &= \begin{bmatrix} G_1\Delta u(t) + f(t+1|t) + \hat{n}(t) \\ G_1\Delta u(t+1) + G_2\Delta u(t) + f(t+2|t) + \hat{n}(t) \\ \vdots \\ G_1\Delta u(t+c-1) + \cdots + G_c\Delta u(t) + f(t+c|t) + \hat{n}(t) \\ \vdots \\ G_1\Delta u(t+p-1) + \cdots + G_p\Delta u(t) + f(t+p|t) + \hat{n}(t) \end{bmatrix}. \end{aligned}$$

The free responses $f(t+k|t)$ and disturbance terms $\hat{n}(t)$ do not depend on current and future step changes. Therefore, the Jacobian of $\hat{\mathbf{y}}(t)$ with respect to $\Delta\mathbf{u}(t)$ has structure $\mathbf{G}$ defined by

$$\mathbf{G} := \frac{\partial\hat{\mathbf{y}}}{\partial\Delta\mathbf{u}} = \begin{bmatrix} G_1 & 0 & 0 & \cdots & 0 \\ G_2 & G_1 & 0 & \cdots & 0 \\ G_3 & G_2 & G_1 & \ddots & \vdots \\ \vdots & \vdots & \vdots & \ddots & 0 \\ G_c & G_{c-1} & G_{c-2} & \cdots & G_1 \\ \vdots & \vdots & \vdots & \vdots & \vdots \\ G_p & G_{p-1} & G_{p-2} & \cdots & G_{p-c+1} \end{bmatrix}. \tag{20}$$

Since $\hat{\mathbf{y}}(t)$ depends linearly on $\Delta\mathbf{u}(t)$, collect a vector of free responses as

$$\mathbf{f}(t) := \mathrm{vec}[f(t+1|t), f(t+2|t), \ldots, f(t+p|t)], \tag{21}$$

and condense the MIMO LTI model predictions into

$$\hat{\mathbf{y}}(t) = \mathbf{G}\Delta\mathbf{u}(t) + \mathbf{f}(t) + 1^p \otimes \hat{n}(t). \tag{22}$$

The globally optimal solution to (18) is the input step change profile $\Delta\mathbf{u}(t)^*$ which evaluates (19) to the zero vector (Nocedal & Wright, 2006). Taking the transpose of (19), assuming W_u and W_y are symmetric,[4] and assuming as in Section 2.3 that y_{sp} is constant for all time t, results in the linear equations

$$\begin{aligned} \left(\frac{\partial\mathcal{J}}{\partial\Delta\mathbf{u}}\right)^\top\Bigg|_{\Delta\mathbf{u}(t)^*} &= 2W_u^\top\Delta\mathbf{u}(t)^* + 2\mathbf{G}^\top W_y^\top(\hat{\mathbf{y}}(t) - 1^p\otimes y_{sp}) \\ &= 2W_u\Delta\mathbf{u}(t)^* + 2\mathbf{G}^\top W_y\big(\mathbf{G}\Delta\mathbf{u}(t)^* \\ &\quad + \mathbf{f}(t) + 1^p\otimes\hat{n}(t) - 1^p\otimes y_{sp}\big) = 0. \end{aligned} \tag{23}$$

[4] Any non-symmetric square weight matrix W producing the quadratic form $x^\top Wx$ may always be re-formulated in symmetric form as $W_s = \frac{1}{2}(W + W^\top)$ to produce an equivalent quadratic form, i.e., $x^\top Wx = x^\top W_s x$.

Denoting the weighting matrix $\mathbf{V} := \left(\mathbf{G}^\top W_y \mathbf{G} + W_u\right)^{-1} \mathbf{G}^\top W_y$ and solving for $\Delta\mathbf{u}(t)^*$ gives

$$\begin{aligned}\Delta\mathbf{u}(t)^* &= -\mathbf{V}\left(\mathbf{f}(t) + 1^p \otimes \hat{n}(t) - 1^p \otimes y_{\text{sp}}\right)\\ &= -\mathbf{V}\left(\mathbf{f}(t) - 1^p \otimes y(t) + 1^p \otimes (y_{\text{m}}(t) - y_{\text{sp}})\right)\\ &= -\mathbf{V}\left(\mathbf{f}(t) - 1^p \otimes f(t|t) - 1^p \otimes e_{\text{curr}}(t)\right),\end{aligned} \tag{24}$$

where $e_{\text{curr}}(t) := y_{\text{sp}} - y_{\text{m}}(t)$ is defined as the current-time measured error from the setpoint. To obtain an expression for the unconstrained QDMC explicit control law $u(t)$, substitute (24) into (10) to obtain

$$\begin{aligned}u(t) = u(t-1) &+ [I_{n_u}\ 0_{n_u}\ \cdots\ 0_{n_u}]\mathbf{V}(1^p \otimes e_{\text{curr}}(t))\\ &- [I_{n_u}\ 0_{n_u}\ \cdots\ 0_{n_u}]\mathbf{V}\left(\mathbf{f}(t) - 1^p \otimes f(t|t)\right).\end{aligned} \tag{25}$$

Next, we show that the controller evolving with (25) contains an integrator in the sense of Lemma 2. Since the third term in (25) consists of only free responses, it depends linearly and only on the previous control actions $u(t-1), u(t-2), \ldots, u(t-N)$. Therefore, we may take the Z-transform of (25) and rearrange terms to obtain $U(z) = K_{\text{QDMC}}(z)E_{\text{curr}}(z)$, where $K_{\text{QDMC}}(z)$ contains an integrator. In order to do so, we require Lemma 4.

Lemma 4. *Extending the current-time free response $f(t|t)$ with future free responses $\mathbf{f}(t)$ gives*

$$\begin{bmatrix} f(t|t) \\ \mathbf{f}(t) \end{bmatrix} = \begin{bmatrix} f(t|t) \\ f(t+1|t) \\ f(t+2|t) \\ \vdots \\ f(t+p|t) \end{bmatrix} = \begin{bmatrix} G_1 & H_2 & \cdots & H_{N-1} & H_N \\ G_2 & H_3 & \cdots & H_N & 0 \\ G_3 & H_4 & \cdots & 0 & 0 \\ \vdots & \vdots & \vdots & \vdots & \vdots \\ G_{p+1} & H_{p+2} & \cdots & 0 & 0 \end{bmatrix} \begin{bmatrix} u(t-1) \\ u(t-2) \\ \vdots \\ \vdots \\ u(t-N) \end{bmatrix}. \tag{26}$$

The reader may intuit the proof of Lemma 4 by noting that, in the free response component (5) of the system output response $\mathbf{y}$ in (1) and (2), control actions do not change after time $t-1$. Theorem 2 is readily obtained from Lemma 4.

Theorem 2. *Consider the LTI predictive model given by (22) and assume that the controller evolution dynamics is governed by (25). Then $K_{\text{QDMC}}(z) = A(z)^{-1}B$, where*

$$B = [I_{n_u}\ 0_{n_u}\ \cdots\ 0_{n_u}]\mathbf{V}(1^p \otimes I_{n_y}) \in \mathbb{R}^{n_u \times n_y} \tag{27}$$

and $A(z) \in \mathbb{R}^{n_u \times n_u}$ is the degree-N matrix polynomial of the variable z^{-1} given by

$$A(z) = \left(I_{n_u} - z^{-1}I_{n_u} - \sum_{i=1}^{N} A_i z^{-i}\right)$$

with $A(1) = 0_{n_u}$.

Proof. The fact that B has the form in (27) follows immediately from (25). To compute polynomial matrix $A(z)$, expand the free response residual between future and current time as

$$\begin{aligned}\mathbf{f}(t) - 1^p \otimes f(t|t) = \Bigg(&\begin{bmatrix} G_2 & H_3 & \cdots & H_N & 0 \\ G_3 & H_4 & \cdots & 0 & 0 \\ \vdots & \vdots & \vdots & \vdots & \vdots \\ G_{p+1} & H_{p+2} & \cdots & 0 & 0 \end{bmatrix}\\ &- 1^p \otimes \begin{bmatrix} G_1 & H_2 & \cdots & H_{N-1} & H_N \end{bmatrix}\Bigg) u_{\text{past}},\end{aligned} \tag{28}$$

where the sequence of all N past inputs is defined by

$$u_{\text{past}} := \text{vec}\left[u(t-1), u(t-2), \cdots, u(t-N)\right]. \tag{29}$$

Applying (28) to the free response terms in (25) and taking the Z-transform gives

$$U(z) = z^{-1}U(z) + BE_{\text{curr}}(z) + \sum_{i=1}^{N} A_i z^{-i} U(z), \tag{30}$$

which has the matrix coefficients

$$\begin{aligned}A_1 &= -[I_{n_u}\ 0_{n_u}\ \cdots\ 0_{n_u}]\mathbf{V}\begin{bmatrix} G_2 - G_1 \\ G_3 - G_1 \\ \vdots \\ G_{p+1} - G_1 \end{bmatrix};\\ A_i &= -[I_{n_u}\ 0_{n_u}\ \cdots\ 0_{n_u}]\mathbf{V}\begin{bmatrix} H_{i+1} - H_i \\ H_{i+2} - H_i \\ \vdots \\ H_{i+p} - H_i \end{bmatrix},\ \forall\, i \geq 2.\end{aligned} \tag{31}$$

Rearranging (30) gives the Z-transform of the structured control law expression

$$U(z) = \left(I_{n_u} - z^{-1}I_{n_u} - \sum_{i=1}^{N} A_i z^{-i}\right)^{-1} BE_{\text{curr}}(z) := A(z)^{-1}BE_{\text{curr}}(z). \tag{32}$$

To show that $A(1) = 0_{n_u}$, we check that $\sum_{i=1}^{N} A_i = 0_{n_u}$. This result is readily derived from the matrix coefficient definitions in (31). Summing from $i = 2$ gives

$$\begin{aligned}\sum_{i=2}^{N} A_i &= -[I_{n_u}\ 0_{n_u}\ \cdots\ 0_{n_u}]\mathbf{V}\begin{bmatrix} -\sum_{i=2}^{2} H_i \\ -\sum_{i=2}^{3} H_i \\ \vdots \\ -\sum_{i=2}^{p+1} H_i \end{bmatrix}\\ &= -[I_{n_u}\ 0_{n_u}\ \cdots\ 0_{n_u}]\mathbf{V}\begin{bmatrix} -(G_2 - G_1) \\ -(G_3 - G_1) \\ \vdots \\ -(G_{p+1} - G_1) \end{bmatrix} = -A_1\end{aligned} \tag{33}$$

by the definition of the step-response coefficient matrices G_i. □

As a corollary to Theorem 1, we can characterize QDMC controller integrator K_{I} using the transfer function $K_{\text{QDMC}}(z)$. Note that $K_{\text{I}} = \lim_{z\to 1}(z-1)K_{\text{QDMC}}(z) = \lim_{z\to 1}(z-1)A(z)^{-1}B$. Assuming that $\lim_{z\to 1}(z-1)A(z)^{-1} = \lim_{z\to 1}((z-1)^{-1}A(z))^{-1}$ exists and is invertible, the computation of the integrator K_{I} can then be found using the L'Hôpital rule. Specifically,

$$K_{\text{I}} = \lim_{z\to 1}((z-1)^{-1}A(z))^{-1}B = \left(I_{n_u} + \sum_{i=1}^{N} iA_i\right)^{-1} B. \tag{34}$$

Therefore, the unconstrained QDMC formulation contains an integrator K_{I} given in (34). Theorem 1 further implies that, when the unconstrained QDMC formulation is applied to the closed-loop system, if the poles of $(I_{n_u} + K_{\text{QDMC}}(z)P(z))^{-1}$ and $(I_{n_u} + K_{\text{QDMC}}(z)P(z))^{-1}P(z)$ lie within the unit circle, and $P(1)K_{\text{I}}$ is invertible, then the controller formulation is offset-free in all n_y performance indices.

Remark 3. Zafiriou (1990) proves robust and nominal asymptotic stability for QDMC controllers with hard input and output constraints, but these proofs often rest on relatively conservative assumptions on the nonlinear state-to-controller mapping and do not guarantee integral action. In the event of controller saturation of the activation of hard state constraints, under constrained QDMC, the state may converge to a new closed-loop equilibrium that deviates from the setpoint. This behavior is illustrated in the simulation results for the first case study shown in Fig. 8.

4. Polynomial chaos expansions and Galerkin projection

This section summarizes PCEs of random variables and Galerkin projection of MIMO LTI systems with parametric uncertainty. Let $(\Omega, \mathcal{F}, \mathbb{P})$ be a probability space and let $\theta \in \Omega \subset \mathbb{R}^n$ be a random variable on Ω representing a vector of parameters with uncertainties. For any measurable square-integrable functions $F : \mathbb{R}^n \to \mathbb{R}$ and $G : \mathbb{R}^n \to \mathbb{R}$,

define the inner product of F and G under the probability measure induced by θ as an expectation over $\mathbb{R}^n$, i.e.,

$$\langle F(\theta), G(\theta)\rangle := \mathbb{E}[F(\theta)G(\theta)] = \int_{\Omega} F(x)G(x)f_\theta(x)\,\mathrm{d}x, \tag{35}$$

where $f_\theta : \mathbb{R}^n \to \mathbb{R}_{\geq 0}$ is the probability density function (PDF). To ensure the validity of PCEs, the probability distribution of the underlying parametric uncertainty θ must satisfy some regularity assumptions. Specifically, θ should be a continuous random variable with sufficiently small tail probabilities to guarantee existence of all moments so that the expectation of any polynomial is well-defined. These assumptions are easily satisfied in many manufacturing and control applications and are summarized in the following assumption:

Assumption 1. We assume that θ satisfies the following conditions (Rahman, 2018)

- θ is an absolutely continuous random variable on $\Omega \subseteq \mathbb{R}^n$ with continuous PDF f_θ.
- θ has bounded moments of all orders, that is,

$$\mathbb{E}[\,|\theta^{\mathbf{j}}|\,] := \int_{\mathbb{R}^n} |x^{\mathbf{j}}| f_\theta(x)dx < \infty \tag{36}$$

  where $\mathbf{j} = (j_1, j_2, \ldots, j_n) \in \mathbb{N}^n$ is a multinomial index with $x^{\mathbf{j}} = x_1^{j_1} x_2^{j_2} \cdots x_n^{j_n}$ and total degree $d := |\mathbf{j}| = \sum_{k=1}^n j_k$.
- f_θ is exponentially integrable, that is, there exists a real-valued scalar $\alpha > 0$ such that[5]

$$\int_{\mathbb{R}^n} e^{-\alpha\|x\|} f_\theta(x)\,\mathrm{d}x < \infty.$$

The first condition is required to prevent the uncertainty structure from being singular, such as those uncertainties having an infinite probability density on measure-zero subsets (e.g., the Dirac delta measure). The second condition is required to ensure that expectations of polynomial functions of θ are well-defined, which is required for the PCE expansions that follow. The third condition is much more technical, but is essential to ensure that θ is uniquely defined by its moments. This highly technical condition is known as the "moment problem" in the literature, and is not entirely crucial for the discussions that follow. The reader is referred to Schmüdgen (2017) for more details.

Intuitively, these assumptions are made to ensure that the modeled parametric uncertainties are well-behaved on the operating space Ω of interest, which is easily verified for many manufacturing applications. For example, if θ has compact support (i.e., the set $\{x \in \mathbb{R}^n \mid f_\theta(x) \neq 0\}$ has a compact closure) and a continuous PDF, then the above assumptions are satisfied. Moreover, if θ is any multivariate Gaussian variable (as is most commonly assumed in process control applications), the above assumptions are immediately satisfied. The components of θ need not be independent, i.e., influences from different parametric uncertainties may be correlated.

If the above assumptions are satisfied, then Theorem 3 holds.

Theorem 3 (*Polynomial Chaos Expansions (Ernst, Mugler, Starkloff, & Ullmann, 2012; Rahman, 2018)*). *Suppose the random parameter θ satisfies Assumption 1, and $y(\theta) \in \mathcal{L}_2(\Omega, \mathcal{F}, \mathbb{P})$ is a real-valued square-integrable system output function of θ. Then there exists a Polynomial Chaos Expansion*

$$y(\theta) = \sum_{k=0}^{\infty} y_k \boldsymbol{\Phi}_k(\theta), \tag{37}$$

where the weighting factors $y_k \in \mathbb{R}^{n_y}$ are deterministic, and each of the $\boldsymbol{\Phi}_k : \mathbb{R}^n \to \mathbb{R}$ are random polynomial basis functions of $\theta \in \Omega$ which are orthonormal with respect to the probability measure induced by θ. That is,

$$\begin{aligned}\langle \boldsymbol{\Phi}_i(\theta), \boldsymbol{\Phi}_j(\theta)\rangle &:= \mathbb{E}[\boldsymbol{\Phi}_i(\theta)\boldsymbol{\Phi}_j(\theta)] \\ &= \int_{\mathbb{R}^n} \boldsymbol{\Phi}_i(x)\boldsymbol{\Phi}_j(x) f_\theta(x)\,\mathrm{d}x = \delta_{i,j},\end{aligned} \tag{38}$$

where $\delta_{i,j} = 1$ for $i = j$; otherwise $\delta_{i,j} = 0$. Furthermore, the (Galerkin) projection of y onto $\boldsymbol{\Phi}_k$ is given by

$$y_k = \langle y, \boldsymbol{\Phi}_k(\theta)\rangle = \int_{\mathbb{R}^n} y(x)\boldsymbol{\Phi}_k(x) f_\theta(x)\,\mathrm{d}x. \tag{39}$$

and the convergence of the expectation of truncated expansion terms of $y(\theta)$ is given in the $\mathcal{L}_2$-sense, i.e.,

$$\begin{aligned}\mathbb{E}\left[\left(y(\theta) - \sum_{k=0}^{K} y_k \boldsymbol{\Phi}_k(\theta)\right)^2\right] &= \int_{\mathbb{R}^n} \left(y(x) - \sum_{k=0}^{K} y_k \boldsymbol{\Phi}_k(x)\right)^2 f_\theta(x)\,\mathrm{d}x \\ &\to 0 \ \text{as}\ m \in \mathbb{N} \to \infty.\end{aligned} \tag{40}$$

In manufacturing applications, the means and variances of uncertain process outputs are of practical interest. By conventions such as in Cameron and Martin (1947) and Xiu and Karniadakis (2002), these vectors may be expressed in the PCT framework by defining $\boldsymbol{\Phi}_0 := 1$, which implies that $\mathbb{E}[\boldsymbol{\Phi}_k(\theta)\boldsymbol{\Phi}_0(\theta)] = \mathbb{E}[\boldsymbol{\Phi}_k(\theta)] = 0$ for $k > 0$. Thereafter, the simple expressions for component-wise means and variances,

$$\mathbb{E}[y(\theta)] = y_0, \qquad \mathrm{Var}[y(\theta)] = \sum_{k=1}^{\infty} y_k^2, \tag{41}$$

are obtained. In the one-dimensional case where $\theta \in \mathbb{R}$, the polynomial basis functions $\boldsymbol{\Phi}_k$ can be indexed by increasing degree due to the natural ordering of $k \in \mathbb{N}$. The polynomial basis functions for some common real-valued random variables are given in Table 1. In the n-dimensional case where $\theta \in \mathbb{R}^n$ and each of the elements θ_j for $j = 1, 2, \ldots, n$ is an independent, identically distributed (i.i.d.) random variable, the polynomial basis functions $\boldsymbol{\Phi}_k(\theta)$ can be taken as the product of the desired basis polynomial for each dimension j. For example, consider the case where θ is a standard Gaussian random vector. The polynomial basis functions are then constructed as products of Hermite polynomials for each θ_j, i.e.,

$$y(\theta) = \sum_{i_1, i_2, \ldots, i_n = 0}^{\infty} y_{i_1, i_2, \ldots, i_n} \prod_{j=1}^{n} \boldsymbol{\Phi}_{i_j}(\theta_j), \tag{42}$$

where $\boldsymbol{\Phi}_k : \mathbb{R} \to \mathbb{R}$ is the kth Hermite polynomial. Moreover, when all components θ_j are i.i.d., the total number of unique expansion terms M is given by the binomial coefficient

$$M = \binom{n+d}{d}, \tag{43}$$

where n is the number of uncertain parameters, and d is the highest total degree of the polynomial functions.[6] Although the number of terms in (43) scales combinatorially as $\mathcal{O}(n^d)$, in practice an accurate representation and propagation of uncertainty can be achieved with a low value of d, e.g., as shown in von Andrian and Braatz (2019, 2020). This property makes PCE a computationally efficient way of incorporating uncertainties of parameters into SMPC, where one must approximate each uncertain parameter as a truncation of the PCE expansion. This approach is known as the Galerkin projection method, which is described in the next section.

[5] This condition implies that the probability of observing very large parametric uncertainties in the nominal process is exceedingly rare and decays quicker than exponentially.

[6] The formula (43) can be observed from a bijection between the number of expansion terms M and the number of ways to arrange d red balls and n blue balls in a line.

Table 1
Some continuous orthogonal basis functions, their commonly used symbols, and associated weight functions $w(x)$ (i.e., scaled forms of probability distributions $f_\theta(x)$ used for quadrature rules Davis & Polonsky, 1972; Petzke, Mesbah, & Streif, 2020) which find use in PCE applications. Populated with reference to Davis and Rabinowitz (1984), Xiu and Karniadakis (2002), and Zelen and Severo (1972). Legendre and Chebyshev polynomials are special cases of Jacobi polynomials, which are included due to their utility in fast spectral and quadrature methods (Boyd, 2001). The support of the distributions is the closure of set $\{x|f_\theta(x) \neq 0\} \subseteq \mathbb{R}^n$. Shape parameters $\alpha > -1$ and $\beta > -1$ are real-valued. Distributions and orthogonal basis functions may be transformed to other supports by affine maps, e.g., the four parameter beta distribution discussed in Couaillier and Savin (2019) is of practical interest. The interested reader may consult (Szegő, 1975) for more details on the theory of classical orthogonal polynomials.

Distribution $f_\theta(x)$	Support x	Polynomial basis functions	Weight function $w(x)$
Uniform	$[-1, 1]$	Legendre $P_n(x)$	1
–	$[-1, 1]$	Chebyshev first kind $T_n(x)$	$(1-x^2)^{-1/2}$
Wigner unit semicircle	$[-1, 1]$	Chebyshev second kind $U_n(x)$	$(1-x^2)^{1/2}$
Transformed beta (Couaillier & Savin, 2019)	$[-1, 1]$	Jacobi $P_n^{(\alpha,\beta)}(x)$	$(1-x)^\alpha(1+x)^\beta$
Unit-rate exponential	$\mathbb{R}_{\geq 0}$	Laguerre $L_n(x)$	$\exp(-x)$
Unit-rate gamma	$\mathbb{R}_{\geq 0}$	Generalized Laguerre $L_n^{(\alpha)}(x)$	$x^\alpha \exp(-x)$
Gaussian	$\mathbb{R}$	Hermite $H_n(x)$	$\exp(-x^2)$

4.1. Galerkin projection method for MIMO LTI systems with parametric uncertainty

Consider the MIMO LTI impulse- and step-response system with parametric uncertainty

$$y(t;\theta) := \sum_{i=1}^{\infty} H_i(\theta)u(t-i) = \sum_{i=1}^{\infty} G_i(\theta)\Delta u(t-i), \tag{44}$$

where each of the $H_i(\theta)$ and $G_i(\theta) = \sum_{j=i}^{\infty} H_j(\theta)$ are parameterized by the random vector $\theta \in \mathbb{R}^n$. In order to ensure that the equality in (44) for a step-response model remains valid, assume that $\sum_{i=1}^{\infty} \|H_i(\theta)\| < M$ almost surely (i.e., with probability one) for some positive real-valued constant $M > 0$. This assumption implies that the corresponding step-response system in (44) is BIBO stable for all possible values of the parametric uncertainty θ. i.e. Now, for any BIBO stable random output response $y(t;\theta)$ depending on random parameter vector θ, Theorem 3 shows that $y(t;\theta) \in \mathcal{L}_2(\Omega, \mathcal{F}, \mathbb{P})$ admits a PCE of form (37). To elucidate the role the temporal dependence plays on the output response in the PCE of $y(t;\theta)$, define the coefficient $y_k(t)$ by applying the Galerkin projection method which involves performing a projection of (44) onto the PCE basis functions $\Phi_k(\theta)$ as in

$$\begin{aligned} y_k(t) &:= \mathbb{E}[y(t;\theta)\Phi_k(\theta)] = \int_{\mathbb{R}^n} \sum_{i=1}^{\infty} H_i(\theta)u(t-i)\Phi_k(\theta)\,\mathrm{d}\theta \\ &= \sum_{i=1}^{\infty}\left(\int_{\mathbb{R}^n} H_i(x)\Phi_k(x)f_\theta(x)\,\mathrm{d}x\right)u(t-i). \end{aligned} \tag{45}$$

Interchanging the integral operator and the infinite summation in (45) follows from the fact that $\sum_{i=1}^{\infty} \|H_i(\theta)\| < M$ almost surely and by dominated convergence. Denoting the (i,k)th inner product of impulse-response coefficient matrices $H_i(\theta)$ and step-response coefficient matrices $G_i(\theta)$ with basis function $\Phi_k(\theta)$ as

$$H_{i,k} := \langle H_i(\theta), \Phi_k(\theta)\rangle = \int_{\mathbb{R}^n} H_i(x)\Phi_k(x)f_\theta(x)\,\mathrm{d}x, \tag{46}$$

and

$$G_{i,k} := \langle G_i(\theta), \Phi_k(\theta)\rangle = \int_{\mathbb{R}^n} G_i(x)\Phi_k(x)f_\theta(x)\,\mathrm{d}x, \tag{47}$$

results in the *non-random* MIMO LTI system for the kth PCE coefficient of $y(t;\theta)$ defined as

$$y_k(t) := \sum_{i=1}^{\infty} H_{i,k}u(t-i) = \sum_{i=1}^{\infty} G_{i,k}\Delta u(t-i). \tag{48}$$

For the purposes of numerical simulation, the expansion must be truncated at some finite order $K \in \mathbb{N}$. By denoting

$$y^{\mathrm{PCE}}(t) := \mathrm{vec}[y_0(t), y_1(t), \ldots, y_{K-1}(t)], \tag{49}$$

$$\begin{aligned} \mathcal{H}_i^{\mathrm{PCE}} &:= \mathrm{vec}[H_{i,0}, H_{i,1}, \ldots, H_{i,K-1}], \\ \mathcal{G}_i^{\mathrm{PCE}} &:= \mathrm{vec}[G_{i,0}, G_{i,1}, \ldots, G_{i,K-1}] \end{aligned} \tag{50}$$

$$= \mathrm{vec}\left[\sum_{j=i}^{\infty} H_{i,0}, \sum_{j=i}^{\infty} H_{i,1}, \ldots, \sum_{j=i}^{\infty} H_{i,K-1}\right], \tag{51}$$

the expanded *non-random* MIMO LTI system containing all the desired PCE coefficients can be written as

$$y^{\mathrm{PCE}}(t) = \sum_{i=1}^{\infty} \mathcal{H}_i^{\mathrm{PCE}}u(t-i) = \sum_{i=1}^{\infty} \mathcal{G}_i^{\mathrm{PCE}}\Delta u(t-i). \tag{52}$$

The mean vector and variance vectors can be approximated by

$$\mathbb{E}[y(t;\theta)] \approx y_0(t), \qquad \mathrm{Var}[y(t;\theta)] \approx \sum_{i=1}^{K-1} y_i(t)^2, \tag{53}$$

where the variance is taken component-wise on the output vector. System (52) for the PCE coefficients can then be used to formulate offset-free QDMC controllers. We develop this key idea in more detail in Section 5.

4.2. Galerkin projections of nonlinear ODEs with parametric uncertainty

Some MIMO process models have a state–space representation with significant nonlinear structure. For such models, expressing the corresponding input–output response model of the form (44) is not analytically tractable, especially in cases where the Galerkin projection integral in (45) does not have a closed form in terms of elementary functions. This subsection describes an approximate method, based on work by Xiu and Karniadakis (2002), for obtaining the PCE step-response coefficient matrices $\mathcal{G}_i^{\mathrm{PCE}}$. Suppose that a system of nonlinear ODEs with uncertain parameters and deterministic input dynamics is modeled by

$$\frac{\mathrm{d}x}{\mathrm{d}t} = f(x, u, \theta), \tag{54}$$

where $t \in \mathbb{R}$ is the continuous time, $x \in \mathbb{R}^{n_x}$ is the state vector, $u \in \mathbb{R}^{n_u}$ is the vector of inputs, and f is some sufficiently smooth but otherwise arbitrary function. Append the linear measurement equations $y(t;\theta) = Cx(t,\theta)$ for some exactly known matrix $C \in \mathbb{R}^{n_y \times n_x}$ to model the random vector of observable quantities $y(t;\theta) \in \mathbb{R}^{n_y}$. Then approximate the dynamics of (54) using the order-P truncated PCE of the state variable x as

$$\frac{\mathrm{d}}{\mathrm{d}t}\left(\sum_{k=0}^{P-1} x_k\Phi_k(\theta)\right) \approx f\left(\sum_{k=0}^{P-1} x_k\Phi_k(\theta), u, \theta\right). \tag{55}$$

An expanded ODE system for PCE coefficients is obtained by the Galerkin projection method:

$$\begin{aligned} \frac{\mathrm{d}x_j}{\mathrm{d}t} &= \left\langle f\left(\sum_{k=0}^{P-1} x_k\Phi_k(\theta), u, \theta\right), \Phi_j(\theta)\right\rangle \\ &= \int_{\mathbb{R}^n} f\left(\sum_{k=0}^{P-1} x_k\Phi_k(\theta), u, \theta\right)\Phi_j(x)f_\theta(x)\,\mathrm{d}x, \end{aligned} \tag{56}$$

where x_j is the jth continuous-time PCE coefficient of the state variable x. The jth continuous-time PCE coefficient of the output variable can be obtained similarly,

$$y_j(t) = C \int_{\mathbb{R}^n} \sum_{k=0}^{P-1} x_k \Phi_k(\theta) \Phi_j(x) f_\theta(x)\, \mathrm{d}x = C x_j(t), \tag{57}$$

which follows immediately from the orthogonality of the polynomial basis $\Phi_k(\theta)$. Similarly to the deterministic case in (2), the step-response coefficient matrices G_i^{PCE} in (52) can be obtained by applying a step input, obtaining the step-response profile of each of the PCE coefficients, and then discretizing the response profile to obtain the step-response coefficients matrices G_i^{PCE}.

5. Offset-free PCE-based QDMC formulations

This section describes three PCE-based QDMC formulations which differ in how the variances of high-order PCE coefficients for process output predictions and observations are weighted in the control objective. The formulations encode different levels of confidence in the model due to parametric uncertainty, making different assumptions regarding the observability of higher order PCE coefficients in the process measurements. For the PCE-based QDMC formulation setting higher order PCE coefficient variance measurements to zero exactly, we also specify necessary and sufficient conditions for nominal and robust stability for unconstrained systems. Much of the notation is re-used from Section 2.3.

Although the three PCE-based QDMC controller formulations differ in the structure of $y_{\mathrm{m}}^{\mathrm{PCE}}(t)$ and $\hat{y}^{\mathrm{PCE}}(t+k|t)$, the formulations continue to retain integrators and offset-free properties under the hypotheses of Theorems 1 and 2. That is, all of the controllers achieve offset-free control for the expected value of each of the multiple performance indices. *The multiple performance indices are interpreted in the PCE-based context to mean an expanded setpoint tracking error* $e^{\mathrm{PCE}}(t+i|t) \in \mathbb{R}^{n_y K}$ *for* $i \in \{1, 2, \dots, p\}$ *in all PCE coefficients of the system output.*

5.1. PCE-based QDMC formulations

PCE-based QDMC shares the same mathematical structure as QDMC presented in Section 2.3, but with one notable difference. First perform a finite-memory truncation of the PCE-based MIMO LTI model (44) to obtain

$$y^{\mathrm{PCE}}(t) = \sum_{i=1}^{N} \mathcal{H}_i^{\mathrm{PCE}} u(t-i) = \sum_{i=1}^{\infty} G_i^{\mathrm{PCE}} \Delta u(t-i), \tag{58}$$

where N is the truncation number determined from system identification procedures. Let $y_{\mathrm{m}}^{\mathrm{PCE}}(t)$ denote the measurement value of y^{PCE}, $\hat{n}^{\mathrm{PCE}}(t+k|t) := y_{\mathrm{m}}^{\mathrm{PCE}}(t) - y^{\mathrm{PCE}}(t)$ denote the disturbance for $k \in \{1, 2, \dots, p\}$, and $\hat{y}^{\mathrm{PCE}}(t+k|t)$ denote the prediction model.[7] Denote the expanded vector of PCE coefficient setpoints as

$$y_{\mathrm{sp}}^{\mathrm{PCE}}(t) := \mathrm{vec}[y_{\mathrm{sp}}(t), 0, \dots, 0]. \tag{59}$$

Essentially, (59) encapsulates the control objective to asymptotically eliminate all higher-moment system output variations — which arise from parametric uncertainty in the system — about a nominal reference signal. In other words, the goal is to stabilize the distribution of system outputs to the deterministically specified setpoints. Letting $e^{\mathrm{PCE}}(t+i|t) := \hat{y}^{\mathrm{PCE}}(t+i|t) - y_{\mathrm{sp}}^{\mathrm{PCE}}(t+i)$, define the modified PCE-based setpoint tracking objective function $\mathcal{J}^{\mathrm{PCE}} \in \mathbb{R}_{\geq 0}$ as

$$\begin{aligned} \mathcal{J}^{\mathrm{PCE}} := &\sum_{i=1}^{p} e^{\mathrm{PCE}}(t+i|t)^\top \mathcal{W}_{yi}^{\mathrm{PCE}} e^{\mathrm{PCE}}(t+i|t) \\ &+ \sum_{i=1}^{c} \Delta u(t+i-1)^\top W_{ui} \Delta u(t+i-1), \end{aligned} \tag{60}$$

where each of the $\mathcal{W}_{yi}^{\mathrm{PCE}} \in \mathbb{R}^{n_y K \times n_y K}$ and $W_{ui} \in \mathbb{R}^{n_u \times n_u}$ is positive semi-definite. In parallel with (8), the convex QP solved by PCE-based QDMC is

$$\begin{aligned} \min_{\mathcal{U}} \quad & \mathcal{J}^{\mathrm{PCE}}(\Delta u(t), \Delta u(t+1), \dots, \Delta u(t+c-1)) \\ \text{s.t.} \quad & A_i^{\mathrm{PCE}} \hat{y}^{\mathrm{PCE}}(t+i|t) \leq b_i, \quad \forall i \in \{1, 2, \dots, p\}, \\ & u_{\min} \leq u(t+i-1) \leq u_{\max}, \quad \forall i \in \{1, 2, \dots, c\}, \\ & \Delta u_{\min} \leq \Delta u(t+i-1) \leq \Delta u_{\max}, \quad \forall i \in \{1, 2, \dots, c\}, \end{aligned} \tag{61}$$

where $\mathcal{U}$ is defined as in (8), $A_i^{\mathrm{PCE}} \in \mathbb{R}^{m \times n_y K}$ carries a sparse structure depending on the controller formulations that follow, and $b_i \in \mathbb{R}^m$ is defined as in (8). Per the discussion in Section 3, the convex and quadratic structure of $\mathcal{J}^{\mathrm{PCE}}$ is due to the PCE-based MIMO LTI model (44) depending linearly and only on past control actions $\mathcal{U}$.

Remark 4. To explicitly include output variances for each of the PCE coefficients in the control objective (60), define

$$\mathcal{W}_{yi}^{\mathrm{PCE}} = \mathrm{diag}[W_{yi}, D, D, \dots, D], \tag{62}$$

where D is a diagonal positive-definite matrix.

As an extension of Section 2.3, simplify the notation for PCE-based QDMC by defining

$$\hat{\mathbf{y}}^{\mathrm{PCE}}(t) := \mathrm{vec}\left[\hat{y}^{\mathrm{PCE}}(t+1|t), \hat{y}^{\mathrm{PCE}}(t+2|t), \dots, \hat{y}^{\mathrm{PCE}}(t+p|t)\right], \tag{63a}$$

$$\mathbf{y}_{\mathrm{sp}}^{\mathrm{PCE}}(t) := \mathrm{vec}\left[y_{\mathrm{sp}}^{\mathrm{PCE}}(t+1), y_{\mathrm{sp}}^{\mathrm{PCE}}(t+2), \dots, y_{\mathrm{sp}}^{\mathrm{PCE}}(t+p)\right], \tag{63b}$$

$$\mathbf{e}^{\mathrm{PCE}}(t) := \hat{\mathbf{y}}^{\mathrm{PCE}}(t) - \mathbf{y}_{\mathrm{sp}}^{\mathrm{PCE}}(t), \tag{63c}$$

$$\mathcal{W}_y^{\mathrm{PCE}} := \mathrm{diag}\left[\mathcal{W}_{y1}^{\mathrm{PCE}}, \mathcal{W}_{y2}^{\mathrm{PCE}}, \dots, \mathcal{W}_{yp}^{\mathrm{PCE}}\right]. \tag{63d}$$

Then, using $\Delta\mathbf{u}(t)$ as defined in (9a), the PCE-based QDMC objective is

$$\mathcal{J}^{\mathrm{PCE}}(\mathbf{e}^{\mathrm{PCE}}(t), \Delta\mathbf{u}(t)) := \mathbf{e}^{\mathrm{PCE}}(t)^\top \mathcal{W}_y^{\mathrm{PCE}} \mathbf{e}^{\mathrm{PCE}}(t) + \Delta\mathbf{u}(t)^\top W_u \Delta\mathbf{u}(t). \tag{63e}$$

Extending (25), the PCE-based QDMC control dynamics evolve according to

$$\begin{aligned} u(t) = u(t-1) &+ [I_{n_u}\ 0_{n_u}\ \cdots\ 0_{n_u}]\, \mathbf{V}^{\mathrm{PCE}}\, (1^p \otimes e_{\mathrm{curr}}^{\mathrm{PCE}}(t)) \\ &- [I_{n_u}\ 0_{n_u}\ \cdots\ 0_{n_u}]\, \mathbf{V}^{\mathrm{PCE}}\, \left(\mathbf{f}^{\mathrm{PCE}}(t) - 1^p \otimes f^{\mathrm{PCE}}(t|t)\right), \end{aligned} \tag{64}$$

where $e_{\mathrm{curr}}^{\mathrm{PCE}}(t) := y_{\mathrm{sp}}^{\mathrm{PCE}} - y_{\mathrm{m}}^{\mathrm{PCE}}(t)$, $f^{\mathrm{PCE}}(t|t)$ is the free response of the prediction model $\hat{y}^{\mathrm{PCE}}$ at the current time, and $\mathbf{f}^{\mathrm{PCE}}(t)$ is the PCE-based vectorization of free responses similar to (21). In addition, the PCE-based weighting matrix $\mathbf{V}^{\mathrm{PCE}}$ and PCE-based overall step-response coefficient matrix $\mathbf{G}^{\mathrm{PCE}}$ are structured as

$$\mathbf{V}^{\mathrm{PCE}} := \left(\mathbf{G}^{\mathrm{PCE}^\top} \mathcal{W}_y^{\mathrm{PCE}} \mathbf{G}^{\mathrm{PCE}} + W_u\right)^{-1} \mathbf{G}^{\mathrm{PCE}^\top} \mathcal{W}_y^{\mathrm{PCE}}, \tag{65}$$

$$\mathbf{G}^{\mathrm{PCE}} := \begin{bmatrix} G_1^{\mathrm{PCE}} & 0 & 0 & \cdots & 0 \\ G_2^{\mathrm{PCE}} & G_1^{\mathrm{PCE}} & 0 & \cdots & 0 \\ G_3^{\mathrm{PCE}} & G_2^{\mathrm{PCE}} & G_1^{\mathrm{PCE}} & \ddots & \vdots \\ \vdots & \vdots & \vdots & \ddots & 0 \\ G_c^{\mathrm{PCE}} & G_{c-1}^{\mathrm{PCE}} & G_{c-2}^{\mathrm{PCE}} & \cdots & G_1^{\mathrm{PCE}} \\ \vdots & \vdots & \vdots & \vdots & \vdots \\ G_p^{\mathrm{PCE}} & G_{p-1}^{\mathrm{PCE}} & G_{p-2}^{\mathrm{PCE}} & \cdots & G_{p-c+1}^{\mathrm{PCE}} \end{bmatrix}. \tag{66}$$

Since (58)–(66) are a reformulation of QDMC for an expanded MIMO LTI system of PCE coefficients, the controller formulation in

[7] Although high-order PCE coefficients are not observable in practice, $y_{\mathrm{m}}^{\mathrm{PCE}}(t)$ may be defined by setting the measured output equal to the zeroth-order PCE coefficient and assuming all higher order coefficients equal zero (see, e.g., (76) below).

(64) always has an integrator. As such, the controllers presented below all contain integrators, with key differences appearing only in (i) the prediction model $\hat{y}^{\text{PCE}}$, (ii) the definition of the measurements $y_{\text{m}}^{\text{PCE}}$, and (iii) the weights corresponding to the higher-order PCE coefficients in the weight matrices $\mathcal{W}_{yi}^{\text{PCE}}$.

5.2. Offset-free controller formulations

5.2.1. PCE-based QDMC with zero-variance weight

The zero-variance weight controller formulation includes only the expected values of system outputs, i.e., the zeroth-order coefficients y_0, in the control objective. Equivalently, all high-order output vector variance weight matrices D_k in (62) are excluded as in

$$\mathcal{W}_{yi}^{\text{PCE}} := \text{diag}[W_{yi},\ 0_{n_y},\ 0_{n_y}, \dots,\ 0_{n_y}]. \tag{67}$$

Simplifying the expressions in (64) and (65) produces a control law that is similar, *but not equivalent*, to the control law (25) previously derived for deterministic QDMC:

$$\begin{aligned} u(t) = u(t-1) &+ [I_{n_u}\ 0_{n_u}\ \cdots\ 0_{n_u}]\mathbf{V}_0(1^p \otimes e_{\text{curr}}(t)) \\ &- [I_{n_u}\ 0_{n_u}\ \cdots\ 0_{n_u}]\mathbf{V}_0\big(\mathbf{f}_0(t) - 1^p \otimes f_0(t|t)\big), \end{aligned} \tag{68}$$

where $\mathbf{f}_0$ is the free response of the zeroth PCE coefficient for all future times $i = 1, 2, \dots, p$, $f_0(t|t)$ is the free response of the zeroth PCE coefficient for the current time. Further, define the weighting matrix for the zeroth-order PCE coefficient,

$$\mathbf{V}_0 := \big(\mathbf{G}_0^\top W_y \mathbf{G}_0 + W_u\big)^{-1}\mathbf{G}_0^\top W_y, \tag{69}$$

where W_y is the weight matrix of the expected value, as defined in (9e). Also, define the step-response coefficient matrix for the zeroth-order PCE coefficient as

$$\mathbf{G}_0 := \begin{bmatrix} G_{1,0} & 0 & 0 & \cdots & 0 \\ G_{2,0} & G_{1,0} & 0 & \cdots & 0 \\ G_{3,0} & G_{2,0} & G_{1,0} & \ddots & \vdots \\ \vdots & \vdots & \vdots & \ddots & 0 \\ G_{c,0} & G_{c-1,0} & G_{1,0} & \cdots & G_{1,0} \\ \vdots & \vdots & \vdots & \vdots & \vdots \\ G_{p,0} & G_{p-1,0} & G_{p-2,0} & \cdots & G_{p-c+1,0} \end{bmatrix}. \tag{70}$$

This formulation has an integrator, because the formulation is a specific case of (64). The advantage of this formulation over the conventional deterministic PCE, which produces control law (25), is that the expected value of the predicted output is used to calculate the setpoint error. The expected value takes into account the entire probability distribution of outputs, which is procedurally different from using a nominal value for the predicted output.

5.2.2. PCE-based QDMC with variance prediction reset to zero at every time step

At every time step t, there exists a measurement of the system $y_m(t)$ indicating that the system has been exactly observed. With this perspective, assume that the higher order PCE coefficients of the free response at the current time, i.e., $f^{\text{PCE}}(t|t) = y(t)$ as defined in Section 2.2, should be set to zero to reflect full certainty in the output value. When the variance prediction is reset to zero at every time step, the PCE-based free response $f^{\text{PCE}}(t+k|t)$ is modified by setting the high-order PCE coefficients as $f_j(t+k|t) = 0$ for $j \in \{1, 2, \dots, K-1\}$. The equation for the predictive model, however, remains unchanged:

$$\hat{y}^{\text{PCE}}(t+k|t) := \sum_{i=1}^{k} \mathcal{G}_i^{\text{PCE}} \Delta u(t+k-i) + f^{\text{PCE}}(t+k|t) + \hat{n}^{\text{PCE}}(t+k|t), \tag{71}$$

where the PCE-based free response is expanded, and the PCE-based disturbance term $\hat{n}^{\text{PCE}}(t+k|t)$ is defined as

$$\begin{aligned} f^{\text{PCE}}(t+k|t) &:= \text{vec}[f_0(t+k|t), f_1(t+k|t), \dots, f_{K-1}(t+k|t)] \\ &= \text{vec}[f_0(t+k|t), 0, \dots, 0], \end{aligned} \tag{72}$$

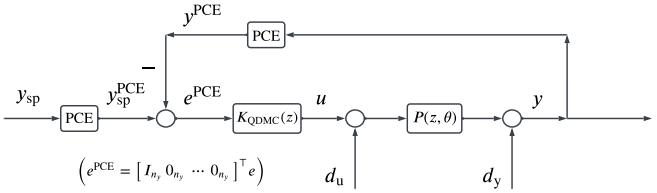

Fig. 2. Block diagram for the closed-loop system with PCE-based QDMC transfer function $K_{\text{QDMC}}(z)$ and parametric uncertainty θ in the plant $P(z,\theta)$. Note that the setpoint error $e(t)$ is not explicitly shown in this block diagram, but we have the projection $e^{\text{PCE}} = [I_{n_y}\ 0_{n_y}\ \cdots\ 0_{n_y}]^\top e(t)$.

$$\hat{n}^{\text{PCE}}(t+k|t) := y_{\text{m}}^{\text{PCE}}(t) - f^{\text{PCE}}(t|t). \tag{73}$$

Simplifying, the predictive model (71)–(73) gives the temporal evolution of the control law as

$$\begin{aligned} u(t) &= u(t-1) - [I_{n_u}\ 0_{n_u}\ \cdots\ 0_{n_u}]\mathbf{V}^{\text{PCE}}(1^p \otimes e_{\text{curr}}(t)) \\ &\quad - [I_{n_u}\ 0_{n_u}\ \cdots\ 0_{n_u}]\mathbf{V}^{\text{PCE}}\big(\mathbf{f}^{\text{PCE}}(t) - 1^p \otimes f^{\text{PCE}}(t|t)\big) \\ &= u(t-1) - [I_{n_u}\ 0_{n_u}\ \cdots\ 0_{n_u}]\mathbf{V}^{\text{PCE}}(1^p \otimes e_{\text{curr}}(t)) \\ &\quad - [I_{n_u}\ 0_{n_u}\ \cdots\ 0_{n_u}]\tilde{\mathbf{V}}\big(\mathbf{f}_0(t) - 1^p \otimes f_0(t|t)\big), \end{aligned} \tag{74}$$

where the weighting matrix is defined by

$$\tilde{\mathbf{V}} := \big(\mathbf{G}^{\text{PCE}^\top}\mathcal{W}_y^{\text{PCE}}\mathbf{G}^{\text{PCE}} + W_u\big)^{-1}\mathbf{G}_0^\top W_y. \tag{75}$$

The controller (74) contains an integrator—the proof essentially follows the same structure as Theorem 2, except with minor modifications. Although (74) is similar to the formulation for zero variance weight in (68), the weight matrix $\tilde{\mathbf{V}}$ has the PCE-based step-response coefficient matrices $\mathbf{G}^{\text{PCE}}$ for high-order coefficients, whereas formulation (69) does not.

Remark 5. In order to determine the value of $e_{\text{curr}}(t)$, the definition for $y_{\text{m}}^{\text{PCE}}(t)$ can be made arbitrary in controller formulation (74), with a canonical definition shown in the next subsection.

5.2.3. PCE-based QDMC with output measurement variance of zero

Accepting that high-order PCE coefficients of the measurements of outputs are not practically observable, the current time output measurements may be assumed to represent the mean output value. That is, the measured value of all higher PCE coefficients is set to zero as in

$$y_{\text{m}}^{\text{PCE}}(t) = \text{vec}[y_{\text{m}}(t), 0, \dots, 0], \tag{76}$$

where $y_{\text{m}}(t)$ is the measured value of the system output at the current time t. This formulation implicitly assumes that all output measurements have a much lower variance compared to the output prediction variance arising from parametric uncertainty alone. Unlike the formulation in Section 5.2.2, the free responses of the higher-order PCE coefficients are not deliberately set to zero—and instead are derived from the MIMO LTI dynamics described by (44). As a result, the controller described here contains an integrator as the controller dynamics follow precisely that of (64). The only modification to (64) is the definition of $y_{\text{m}}^{\text{PCE}}(t)$ using (76), which also influences $e_{\text{curr}}^{\text{PCE}}(t)$.

5.3. Nominal and robust stability for zero output measurement variance controller

We proceed to specify sufficient conditions for nominal and robust stability for the controller formulation in Section 5.2.3. Corresponding conditions for the remaining controller formulations in Sections 5.2.1 and 5.2.2 may be specified similarly. Consider the closed-loop feedback structure in Fig. 2. The MIMO LTI plant with parametric uncertainty $P(z,\theta)$ takes the disturbed control signal $u(t)$ and outputs the disturbed

signal $y(t)$, which not yet expanded into PCE coefficients. The output $y(t)$ is fed back as the measurement $y_{\mathrm{m}}(t)$, which is expanded into the PCE-based measured output $y_{\mathrm{m}}^{\mathrm{PCE}}(t)$ given by (76), which is finally compared as an error against the PCE setpoint value $y_{\mathrm{sp}}^{\mathrm{PCE}}(t)$ given in (59). The controller transfer function $K_{\mathrm{QDMC}}(z)$ represents the PCE-based control law in (64), and the plant transfer function $P(z,\theta)$ represents the transfer function of the MIMO LTI system with uncertain parameters θ. The nominal MIMO LTI plant $P_0(z)$ can be viewed as the MIMO LTI system formed by a nominal realization of the random variable θ. We herein define $P_0(z) := P(z,\theta_0)$ for some $\theta_0 \in \operatorname{supp}\theta$, where supp θ denotes the support of θ. The output measurement $y_{\mathrm{m}}(t)$ and setpoint $y_{\mathrm{sp}}(t)$ have the zero-variance PCE projections

$$y_{\mathrm{m}}^{\mathrm{PCE}}(t) = \begin{bmatrix} I_{n_y} \\ 0 \\ \vdots \\ 0 \end{bmatrix} y_{\mathrm{m}}(t)\,, \quad y_{\mathrm{sp}}^{\mathrm{PCE}}(t) = \begin{bmatrix} I_{n_y} \\ 0 \\ \vdots \\ 0 \end{bmatrix} y_{\mathrm{sp}}(t)\,, \tag{77}$$

We have $e_{\mathrm{curr}}^{\mathrm{PCE}}(t) = y_{\mathrm{m}}^{\mathrm{PCE}}(t) - y_{\mathrm{sp}}(t)$, and defining the PCE-based QDMC controller transfer function projection as

$$\tilde{K}(z) := K_{\mathrm{QDMC}}(z) \begin{bmatrix} I_{n_y} \\ 0 \\ \vdots \\ 0 \end{bmatrix}, \tag{78}$$

leads up to Theorem 4 on nominal closed-loop stability:

Theorem 4 (*Nominal Stability*)**.** *Consider the input- and output-disturbed closed-loop feedback system in Fig. 2 with the PCE-based controller $K_{\mathrm{QDMC}}(z)$ and nominal MIMO LTI plant $P_0(z) = P(z,\theta_0)$. Then the Z-transform of the non-expanded setpoint error $e(t) = y(t) - y_{\mathrm{sp}}(t) \in \mathbb{R}^{n_y}$ is*

$$E(z) = \left(I_{n_y} + P_0(z)\tilde{K}(z)\right)^{-1}\left(-Y_{\mathrm{sp}}(z) + D_y(z) + P_0(z)D_u(z)\right), \tag{79}$$

where $\tilde{K}(z)$ is given in (78), $K_{\mathrm{QDMC}}(z) = A(z)^{-1}B$ and $A(1) = 0_{n_u}$, as in Theorem 2. We obtain, in parallel with Theorem 2, the temporal evolution contribution of the control law as

$$B = [I_{n_u}\ 0_{n_u}\ \cdots\ 0_{n_u}]\,\mathbf{V}^{\mathrm{PCE}}\,(1^p \otimes I_{n_y K}), \tag{80}$$

and the degree-N matrix polynomial $A(z)$ specified by matrix coefficients A_i as

$$A(z) = \left(I_{n_u} - z^{-1}I - \sum_{i=1}^{N} A_i z^{-i}\right), \tag{81}$$

$$A_1 = -[I_{n_u}\ 0_{n_u}\ \cdots\ 0_{n_u}]\mathbf{V}^{\mathrm{PCE}} \begin{bmatrix} \mathcal{G}_2^{\mathrm{PCE}} - \mathcal{G}_1^{\mathrm{PCE}} \\ \mathcal{G}_3^{\mathrm{PCE}} - \mathcal{G}_1^{\mathrm{PCE}} \\ \vdots \\ \mathcal{G}_{p+1}^{\mathrm{PCE}} - \mathcal{G}_1^{\mathrm{PCE}} \end{bmatrix}, \tag{82}$$

$$A_i = -[I_{n_u}\ 0_{n_u}\ \cdots\ 0_{n_u}]\mathbf{V}^{\mathrm{PCE}} \begin{bmatrix} \mathcal{H}_{i+1}^{\mathrm{PCE}} - \mathcal{H}_i^{\mathrm{PCE}} \\ \mathcal{H}_{i+2}^{\mathrm{PCE}} - \mathcal{H}_i^{\mathrm{PCE}} \\ \vdots \\ \mathcal{H}_{i+p}^{\mathrm{PCE}} - \mathcal{H}_i^{\mathrm{PCE}} \end{bmatrix}, \quad \forall i \geq 2. \tag{83}$$

In particular, if $P_0(1)K_{\mathrm{I}}$ in $\tilde{K}(z)$ is invertible and all poles of $-\left(I_{n_y} + P_0(z)\tilde{K}(z)\right)^{-1}$ and $-\left(I_{n_y} + P_0(z)\tilde{K}(z)\right)^{-1}P_0(z)$ lie within the unit circle, then the nominal closed-loop system with the PCE-based controller is closed-loop stable and offset-free for unconstrained systems.

Proof. Follows readily from Theorem 2. Specifically, the impulse and step response coefficients H_i and G_i in Theorem 2 are substituted with the expanded PCE impulse and step response coefficients $\mathcal{H}_i^{\mathrm{PCE}}$ and $\mathcal{G}_i^{\mathrm{PCE}}$ from the PCE-expanded model in Eq. (58). □

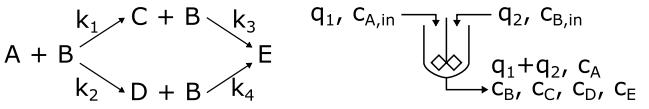

Fig. 3. Series–parallel reaction network and CSTR configuration studied. All reaction rate laws are bilinear in species concentrations. Species C is the desired high-value product produced by reaction rate constant k_1, but all other reactions lower the selectivity to species C. Only inlet stream 1 volumetric flow rate q_1 may be manipulated, e.g., with a valve.
Source: Re-printed with permission from von Andrian and Braatz (2020).

Similarly, a sufficient condition for robust stability can be formulated by noting that the uncertainty is described by the random variable θ and, if the controller renders the system closed-loop stable and offset-free for all possible values of θ, then the controller is also robustly stable. This is summarized in the following corollary:

Corollary 1 (*Robust Stability*)**.** *Consider the input- and output-disturbed closed-loop system in Fig. 2 with the PCE-based controller $K_{\mathrm{QDMC}}(z)$. The system is closed-loop stable and offset-free with probability one if $P(1,\theta)K_{\mathrm{I}}$ is invertible and all poles of $-\left(I_{n_y} + P(z,\theta)\tilde{K}(z)\right)^{-1}$ lie within the unit circle with probability one.*

6. Case study 1: Offset-free control of product concentration in a reaction network

This section evaluates the effectiveness of PCE-based QDMC formulations in providing offset-free control to the manufacturing of a pharmaceutical intermediate in a continuously stirred tank reactor (CSTR). The case study is adapted from a series–parallel nucleophilic aromatic substitution reaction network (Reizman & Jensen, 2012). Such networks describe multi-step synthetic routes where selectivity towards the high-value product in a series reaction is lowered by side-product formation in parallel reactions. The model parameters for this process have high parametric uncertainty (Reizman & Jensen, 2012; Shen & Braatz, 2016).

More specifically, the reaction network and CSTR configuration summarized in Fig. 3 are numerically simulated. The network consists of five chemical species and four reactions. Each reaction rate law is modeled as a single rate constant parameter multiplying a second-order, bilinear structure in the reacting species concentrations. With continuous ideal mixing and removal, the dynamic operation of the CSTR is modeled as the random nonlinear ODE system

$$\frac{\mathrm{d}c_{\mathrm{A}}}{\mathrm{d}t} = \frac{q_1}{V}c_{\mathrm{A,in}} - c_{\mathrm{A}}\frac{q_1+q_2}{V} - c_{\mathrm{A}}c_{\mathrm{B}}(k_1+k_2), \tag{84a}$$

$$\frac{\mathrm{d}c_{\mathrm{B}}}{\mathrm{d}t} = \frac{q_2}{V}c_{\mathrm{B,in}} - c_{\mathrm{B}}\frac{q_1+q_2}{V} - c_{\mathrm{A}}c_{\mathrm{B}}(k_1+k_2) \tag{84b}$$

$$- c_{\mathrm{B}}c_{\mathrm{C}}k_3 - c_{\mathrm{B}}c_{\mathrm{D}}k_4, \tag{84c}$$

$$\frac{\mathrm{d}c_{\mathrm{C}}}{\mathrm{d}t} = -c_{\mathrm{C}}\frac{q_1+q_2}{V} + c_{\mathrm{A}}c_{\mathrm{B}}k_1 - c_{\mathrm{B}}c_{\mathrm{C}}k_3, \tag{84d}$$

$$\frac{\mathrm{d}c_{\mathrm{D}}}{\mathrm{d}t} = -c_{\mathrm{D}}\frac{q_1+q_2}{V} + c_{\mathrm{A}}c_{\mathrm{B}}k_2 - c_{\mathrm{B}}c_{\mathrm{D}}k_4, \tag{84e}$$

where c_i is the concentration of species $i = \{\mathrm{A,B,C,D,E}\}$, $c_{i,\mathrm{in}}$ is the inlet stream concentration of c_i, q_1 and q_2 are the total volumetric flow rates of inlet streams 1 and 2, and k_j is the rate constant for reaction $j = \{1,2,3,4\}$. In all numerical simulations, the rate constants k_1 and k_2 are uniformly distributed over the non-random intervals $[k_{1,\min}, k_{1,\max}]$ and $[k_{2,\min}, k_{2,\max}]$, respectively. Rate constants k_3 and k_4 are specified deterministically, e.g., the rate constants may have been estimated well from previous experiments. Table 2 describes all non-random, time-invariant parameters used in numerically simulating (84).

For closed-loop simulations, the manipulated variable is q_1, which contains species A. A manufacturing performance specification is given on the desired product, i.e., a concentration setpoint $c_{\mathrm{C,sp}}$ placed on

Table 2
Non-random time-invariant parameters used in simulating (84). Adapted from von Andrian and Braatz (2020) with modifications to $k_{1,\text{nom}}$, $k_{2,\text{nom}}$, $c_{A,\text{in}}$, k_3, k_4, and steady-state operating conditions. The manipulated variable q_1 is not specified since it may be any positive, real-valued, bounded input time series into the reactor.

System parameter	Description	Nominal value	Units
$k_{1,\min}$	Minimal rate constant 1	0.2789	L/mol-s
$k_{1,\max}$	Maximal rate constant 1	0.8927	L/mol-s
$k_{1,\text{nom}}$	Nominal rate constant 1	0.5858	L/mol-s
$k_{2,\min}$	Minimal rate constant 2	0.1894	L/mol-s
$k_{2,\max}$	Maximal rate constant 2	0.9331	L/mol-s
$k_{2,\text{nom}}$	Nominal rate constant 2	0.56125	L/mol-s
k_3	Reaction rate constant 3	3.264	L/mol-s
k_4	Reaction rate constant 4	0.01591	L/mol-s
V	CSTR volume	5	L
q_2	Inlet 2 volumetric flow rate	1	L/s
$c_{A,\text{in}}$	Inlet A concentration	0.3	mol/L
$c_{B,\text{in}}$	Inlet B concentration	7.35	mol/L
$c_{A,\text{ss}}$	Steady-state concentration of A	0.06044	mol/L
$c_{B,\text{ss}}$	Steady-state concentration of B	1.72578	mol/L
$c_{C,\text{ss}}$	Steady-state concentration of C	0.00957	mol/L
$c_{D,\text{ss}}$	Steady-state concentration of D	0.07531	mol/L
$q_{1,\text{ss}}$	Steady-state inlet 1 flow rate	2.75	L/s
$c_{A,0}$	Initial concentration of A	0	L/mol
$c_{B,0}$	Initial concentration of B	3.5	L/mol
$c_{C,0}$	Initial concentration of C	0	L/mol
$c_{D,0}$	Initial concentration of D	0.0025	L/mol

the outlet concentration of species C. The control variable c_C is directly measured without error. For a fixed nominal value of inlet 1 flow rate $q_{1,\text{ss}}$, the system (84) has an equilibrium point at $[c_{A,\text{ss}}, c_{B,\text{ss}}, c_{C,\text{ss}}, c_{D,\text{ss}}]^\top$ (which can be found by a nonlinear equation solver), and the exact coordinates of this equilibrium point are provided in Table 2. The control inputs and output responses are expressed in terms of deviation variables as $u = q_1 - q_{1,\text{ss}}$ and $y := c_C - c_{C,\text{ss}}$, respectively.

6.1. Non-random ODE system generation by PCE

In all numerical simulations, define the non-random, nominal values $k_{1,\text{nom}} := \frac{1}{2}(k_{1,\min} + k_{1,\max})$ and $k_{2,\text{nom}} := \frac{1}{2}(k_{2,\min} + k_{2,\max})$ and rescale k_1 and k_2 by two i.i.d. random variables θ_1 and θ_2 as uniform distributions with support $\theta_1, \theta_2 \in [-1, 1]$, i.e., we denote $\theta_1, \theta_2 \sim U([-1, 1])$, by applying the linear and invertible change of variables

$$k_1 = \frac{k_{1,\min} + k_{1,\max}}{2} + \frac{k_{1,\min} - k_{1,\max}}{2}\theta_1, \tag{85a}$$

$$k_2 = \frac{k_{2,\min} + k_{2,\max}}{2} + \frac{k_{2,\min} - k_{2,\max}}{2}\theta_2. \tag{85b}$$

For $\theta_1, \theta_2 \sim U([-1, 1])$, Table 1 indicates that Legendre polynomials are the appropriate PCE basis set to use. We choose a fourth-order expansion on the two random parameters, i.e., $d = 4$ and $n = 2$ in (43), to expand each species c_i into $M = 15$ distinct coefficients $c_{i,j,k}$ as

$$c_i = \sum_{\substack{j,k \\ j+k\le 4}} c_{i,j,k}\Phi_j(\theta_1)\Phi_k(\theta_2), \tag{86}$$

where Φ_j is the Legendre polynomial of degree j. The temporal evolution of PCE coefficients is then numerically computed by (i) substituting (86) into the ODE system (84), (ii) performing Galerkin projections as described in Section 4.2, and (iii) numerically integrating the expanded ODE system totaling 60 PCE coefficients. We apply the Polynomial Chaos Expansion Toolbox (PoCET) (Petzke et al., 2020), which uses symbolic algebra for computing the Galerkin projection integrals in Step 2. Assume that the initial state vector is non-random, so all the nonzero-order PCE coefficients for the expanded initial state vector are chosen to be zero exactly.

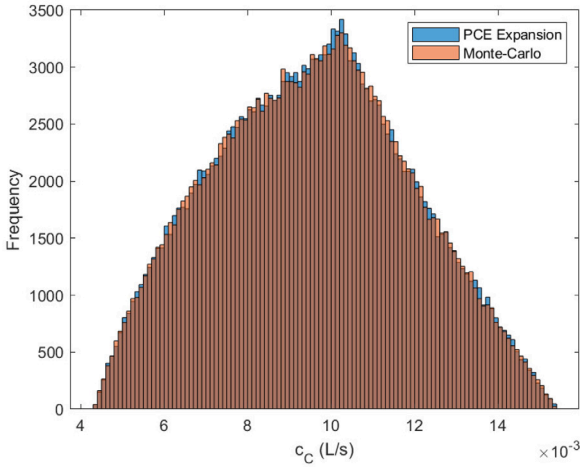

Fig. 4. Histograms for 100 000 random samples of c_C at 40 s generated by Monte Carlo simulations (orange) and expanded PCE coefficient ODE system (blue). (For interpretation of the references to color in this figure legend, the reader is referred to the web version of this article.)

6.2. Benchmarking forward uncertainty propagation with Monte Carlo sampling

To benchmark the accuracy of the PCE approximations to the system dynamics in (84), Monte Carlo simulations are performed by solving the ODE system for various random sample draws of k_1 and k_2 using $\theta_1, \theta_2 \sim U([-1, 1])$ and the transformations (85). Monte Carlo sampling is a computationally expensive but highly accurate approximation to the temporally evolving probability distribution of c_C. The sampling approach has been shown as an appropriate benchmark to use in other numerical studies (Kim, Shen, Nagy, & Braatz, 2013; von Andrian & Braatz, 2020).

With the Monte Carlo sampling approach, for an initial charge $[c_{A,0}, c_{B,0}, c_{C,0}, c_{D,0}]^\top$ and no control action and input/output disturbances, i.e., $q_1 = q_{1,\text{ss}}$, $q_2 = 0$, the ODEs in (84) are solved for various sampled parameters $\{k_1, k_2\}$ to obtain an approximate probability distribution for c_C at 40 s. An initial state vector for the Monte Carlo approach is used to solve (84) that holds the same values as the zeroth-order PCE coefficient of the expanded initial state vector. In comparison, solution of the expanded ODE system produces a time-varying set of PCE coefficients for c_C which induce an approximate probability distribution for c_C under the Legendre polynomial basis. The distribution of c_C is then approximated by sampling various values of $\{\theta_1, \theta_2\}$ and applying the PCE transform in the sense of Theorem 3 and (37).

The histograms for c_C at 40 s using the Monte Carlo sampling-simulated distribution and the PCE-approximated distribution are compared in Fig. 4. The histograms show negligible difference in the shapes of the probability distribution, and the relative error between the variance of the PCE-approximated distribution and the variance of Monte Carlo benchmark is 0.58%. This comparison demonstrates that PCE-expanded model has high numerical accuracy when propagating uncertainty forward for the CSTR.

6.3. Open-loop analysis problem: Input-output response disturbance-free system identification

By numerical time integration of expanded ODE system for the PCE coefficients using `ode45` in MATLAB version R2023b (The MathWorks Inc., 2023), disturbance-free input–output response model identification is performed by first applying a unit step-response $u = 1$ L/s to the nominal open-loop system (84). The step response for each of the PCE

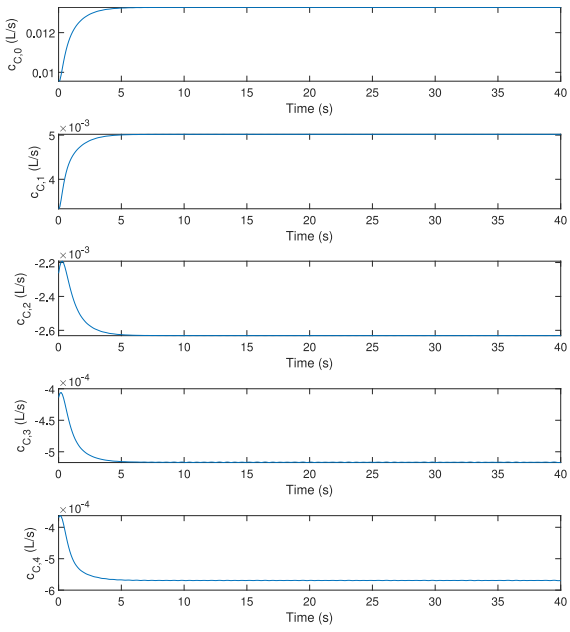

Fig. 5. The first five PCE coefficient values of c_C as they vary in time. All PCE coefficients are observed to stabilize after 10 s.

Table 3
Non-random time-invariant parameters used in simulating (89) and (90).

System parameter	Description	Nominal value	Units
k_{nom}	Nominal heat transfer coefficient	1	1/s
Δ_1	Uncertainty level for k_{ij}	$\sqrt{3}/10$	–
Δ_2	Uncertainty level for η_2	$\sqrt{3}/10$	–
$\bar{d}$	Average distance between nodes	0.1068	m
η_1	Loss coefficient for heat exchange with the environment	1	1/s
$\eta_{2,nom}$	Nominal actuator gain constant	1	K/s

coefficients of c_C is then observed to stabilize after approximately 10 s, see Fig. 5. The truncation number N is set as the total time to stabilize divided by the constant output sampling time frequency Δt, as given in Table 4. Plots of the output response of the first five PCE coefficients of c_C are shown in Fig. 5. With output responses measured, the PCE-based step-response coefficient matrices $\mathcal{G}_i^{PCE}$ given by (51) are computed for the step-response MIMO LTI system in (58).

6.4. Closed-loop synthesis problem: PCE-based QDMC performance

The MATLAB QDMC package (von Andrian-Werburg, 2024) is used to solve the controller formulation

$$\begin{aligned}\mathcal{J}^{PCE} := &\sum_{i=1}^{p} e^{PCE}(t+i|t)^\top \mathcal{W}_y^{PCE} e^{PCE}(t+i|t) \\ &+ \sum_{i=1}^{c} \Delta u(t+i-1)^\top W_u \Delta u(t+i-1),\end{aligned} \tag{87}$$

$$\begin{aligned}\min_{\mathcal{U}} \quad & \mathcal{J}^{PCE}(\Delta u(t), \Delta u(t+1), \dots, \Delta u(t+c-1)) \\ \text{s.t.} \quad & y_{min}^{PCE} \le \hat{y}^{PCE}(t+i|t) \le y_{max}^{PCE}, \quad \forall i \in \{1,2,\dots,p\}, \\ & u_{min} \le u(t+i-1) \le u_{max}, \quad \forall i \in \{1,2,\dots,c\}, \\ & \Delta u_{min} \le \Delta u(t+i-1) \le \Delta u_{max}, \quad \forall i \in \{1,2,\dots,c\},\end{aligned} \tag{88}$$

at each discrete sampling time t, where $\mathcal{U}$ is defined as in (8). All control parameters used for closed-loop numerical simulations, such as the prediction horizon p and control horizon c, are provided in Table 4. The expressions for the weight matrices $\mathcal{W}_y^{PCE}$ and W_u, and the output

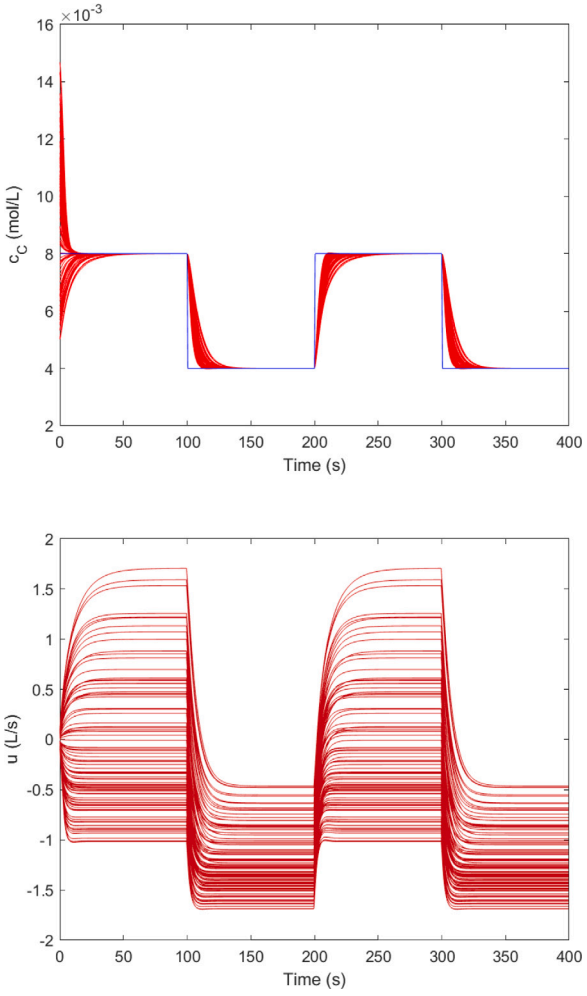

Fig. 6. Top: Closed-loop responses (red) for c_C for 100 realizations of the random rate constants k_1 and k_2. With no input and output disturbances and several step changes in the setpoint at times $t_{sp} \in \{100, 200, 300\}$ s, all trajectories of c_C quickly reach $c_{C,sp}$ (blue) with effectively zero offset. Bottom: Corresponding control trajectories. (For interpretation of the references to color in this figure legend, the reader is referred to the web version of this article.)

constraint vectors y_{min}^{PCE} and y_{max}^{PCE}, are relatively large in size and are provided in the MATLAB code in the Github repository. The coefficient matrices $\mathcal{G}_i^{PCE}$ identified in the previous subsection are used for the predictive model $\hat{y}^{PCE}(t+i|t)$.

In order to evaluate the performance of the PCE-based QDMC strategy, closed-loop simulations of the system are performed using a performance index for setpoint tracking of the concentration c_C. In the closed-loop simulations, the setpoint $c_{C,sp}$ is stepped up and down every 100 s, and the goal is to perform setpoint tracking for the desired output c_C. Fig. 6 plots the output responses for 100 random samples of k_1 and k_2. The closed-loop responses show that PCE-based QDMC is able to perform robust setpoint tracking.

To show that the PCE-based QDMC controller performs well in the presence of input and output disturbances, additional two separate closed-loop simulations are performed, one with a moderate input disturbance of $d_u = \pm 0.5$ L/s and one with a large output disturbance of $d_y = \pm 0.003$ mol/L. The results are shown in Fig. 7 for the input disturbance, and Fig. 8 for the output disturbance. Critically, insofar as the input constraints are not active, the responses shows excellent disturbance rejection. Fig. 8 indicates that, for several samples of $\{\theta_1, \theta_2\}$, the output is not offset-free for the second disturbance due to control constraints being too tight. The system response is bounded, which

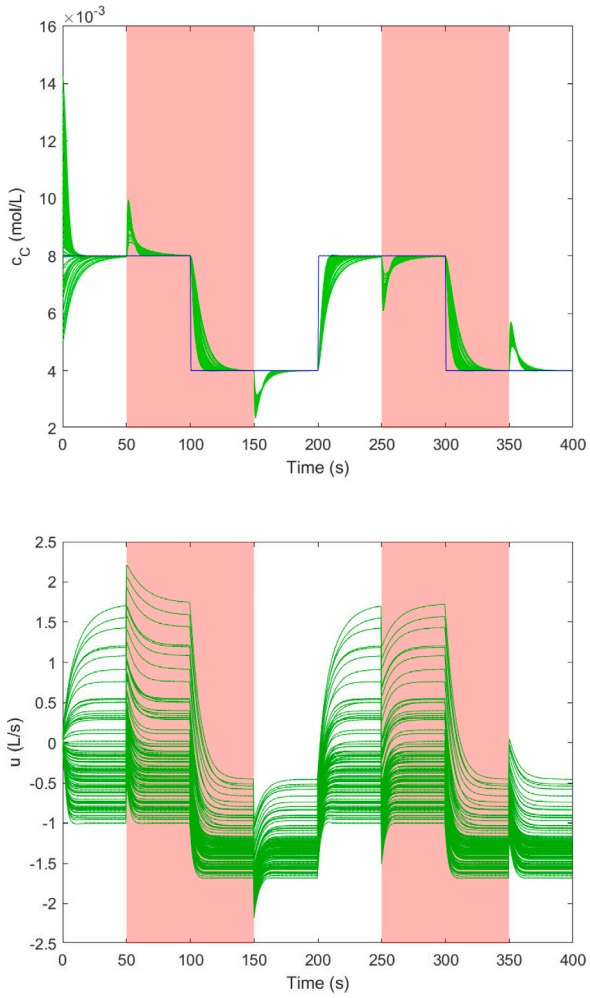

Fig. 7. Top: Closed-loop responses (green) for c_C for 100 realizations of the random rate constants k_1 and k_2, and two constant input disturbances (red): the first at $d_u = 0.5$ L/s for $t \in [50, 150]$ s, and the second at $d_u = -0.5$ L/s for $t \in [250, 350]$ s. Under several changes in the setpoint at times $t_{sp} \in \{100, 200, 300\}$ s, all trajectories of c_C quickly reach $c_{C,sp}$ (blue) with effectively zero offset. Bottom: Corresponding control trajectories, with notable spikes at $t = 50$, 150, 250, and 350 s, which are the junctures where there is a discontinuous change in the disturbance d_u. (For interpretation of the references to color in this figure legend, the reader is referred to the web version of this article.)

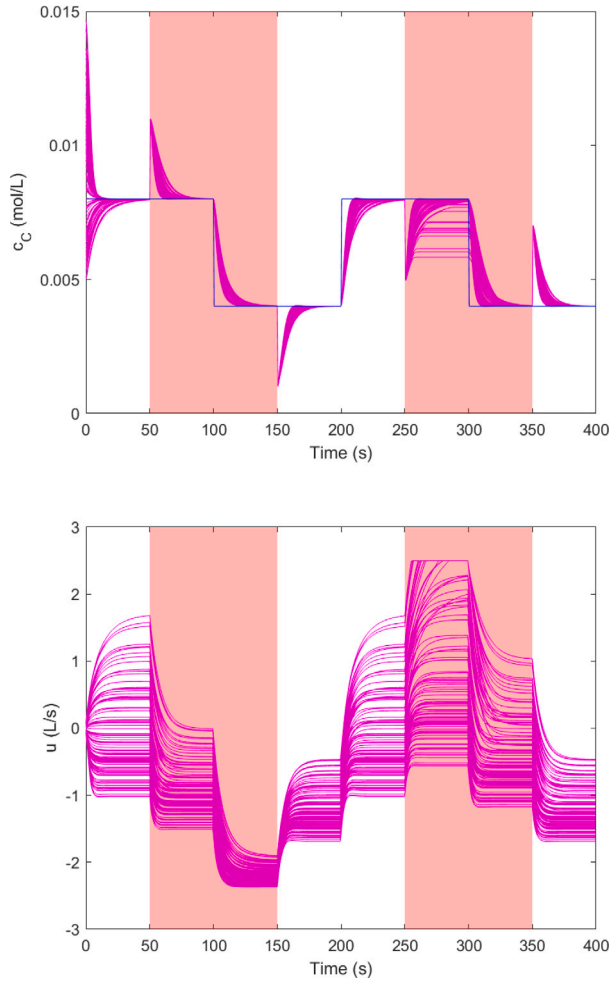

Fig. 8. Top: Closed-loop responses (magenta) for c_C for 100 realizations of the random rate constants k_1 and k_2, and two constant output disturbances (red): the first at $d_y = 0.003$ mol/L for $t \in [50, 150]$ s, and the second at $d_y = -0.003$ mol/L for $t \in [250, 350]$ s. Under several changes in the setpoint at times $t_{sp} \in \{100, 200, 300\}$ s, most trajectories of c_C quickly reach the setpoint (blue) with effectively zero offset. In some cases, the controller constraints are not wide enough and there are no feasible input actions to asymptotically remove offset in the system at the second output fault. Additional simulations show that relaxing to $u_{min} = -3$ and $u_{max} = 3$ removes these feasibility issues. Bottom: Corresponding control trajectories, with notable actuator saturation at $u = 2.5$ for some realizations of k_1 and k_2. These control trajectories correspond to the output trajectories with non-zero offset and where the input constraints are active. (For interpretation of the references to color in this figure legend, the reader is referred to the web version of this article.)

is consistent with the closed-loop system being BIBO stable. When the input constraints are relaxed, offset-free responses are observed. These closed-loop performance outcomes are attributable to the PCE-based controller formulation containing an integrator, which in turn ensures that the closed-loop rejects plant input and output disturbances during setpoint tracking.

7. Case study 2: Thermal regulation on the IEEE 118-bus network

To further evaluate the effectiveness of PCE-based QDMC in providing offset-free regulation, consider the thermal regulation problem on the IEEE 118-Bus Network (Zimmerman, Murillo-Sánchez, & Thomas, 2010), which is a standardized benchmark for evaluating control algorithms on large-scale networked systems where the topology of the network graph directly affects the system dynamics. In this study, each of the 118 buses is considered a node in an undirected graph, and the edges represent a channel for direct heat transfer between nodes, so heat transfer can only occur if and only if there is an edge connecting the two nodes. Fig. 9 shows the IEEE 118-bus graph network's topology, where the nodes are grouped into different clusters, each represented by a different color. The graph is simple and does not contain any self-loops. The dynamics of the system are governed by the Laplacian-like ODE:

$$\frac{\mathrm{d}T_i}{\mathrm{d}t} = -\sum_{j \in \mathcal{N}_i} k_{ij}(T_i - T_j) - \eta_1 T_i + \eta_2 u_i, \tag{89}$$

where $\mathcal{N}_i$ is the set of nodes connected to node i by an edge, T_i is the temperature (in deviation variables) of the node i, k_{ij} is thermal coupling coefficient between node i and j, and $\eta_1 > 0$ is a positive constant which governs the rate of local heat loss, and η_2 is a positive constant governing heat generation term, and u_i is the control input at node i. The thermal coupling coefficients k_{ij} and the heat generation constant η_2 are uncertain parameters defined as

$$k_{ij} := k_{\text{nom}} \frac{\bar{d}}{d_{ij}}(1 + \theta_1 \Delta_1), \tag{90a}$$

$$\eta_2 := \eta_{2,\text{nom}}(1 + \theta_2 \Delta_2), \tag{90b}$$

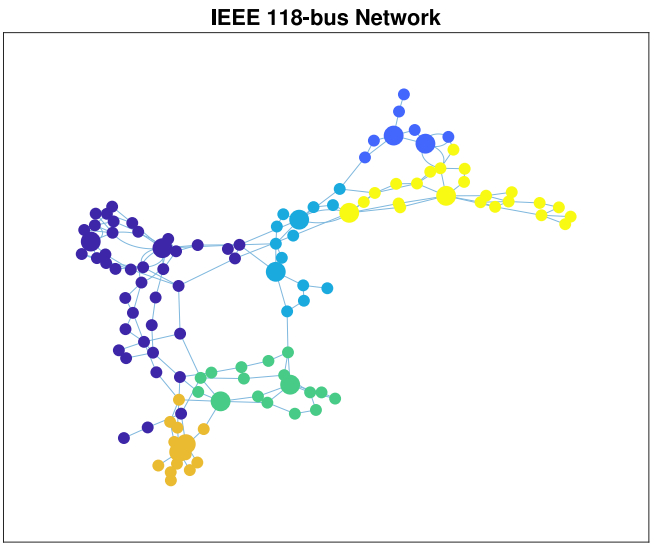

Fig. 9. Graph topology of the IEEE 118-bus network system, with each node assigned a color representing its cluster assignment. Enlarged nodes represent nodes where a control action was actuated. (For interpretation of the references to color in this figure legend, the reader is referred to the web version of this article.)

Table 4
Controller parameters used in PCE-based QDMC closed-loop simulations of (84). "s.s". signifies "steady state". Adapted from von Andrian and Braatz (2020) with modifications to Δt, N, p, and input and output constraints. Weight matrices $\mathcal{W}_y^{\text{PCE}}$ and W_u, and extended output constraint vectors $y_{\min}^{\text{PCE}}$ and $y_{\max}^{\text{PCE}}$, are all provided in the MATLAB files available at Github.

Controller parameter	Description	Nominal Value	Units
Δt	Sampling time step	0.5	s
N	Model truncation number	20	–
p	Prediction horizon length	20	–
c	Control horizon length	5	–
$u_{\min}$	Minimum inlet 1 flow rate deviation from s.s.	−2.5	L/s
$u_{\max}$	Maximum inlet 1 flow rate deviation from s.s.	2.5	L/s
$\Delta u_{\min}$	Minimum inlet 1 flow rate decrease	−0.1	L/s
$\Delta u_{\max}$	Maximum inlet 1 flow rate increase	0.1	L/s
$y_{\min}$	Minimum measurable species C concentration	−0.02	mol/L
$y_{\max}$	Maximum measurable species C concentration	0.02	mol/L

where θ_1 and θ_2 are uniformly distributed independent variables on the interval $[-1,1]$, $\bar{d}$ is the average length of the edges in the graph, d_{ij} is the length of the edge connecting nodes i and j, Δ is a parameter representing the degree of uncertainty in the parameters, and k_{nom} is a nominal value for the coupling coefficient. Intuitively, (90a) models the fact that, for conductive heat transfer, the effective resistance is directly proportional to the thermal conductivity and inversely proportional to the distance between the nodes. The constant and Δ_1 and Δ_2 represent the degree of parametric uncertainty in the model. Table 3 describes all non-random, time invariant parameters for the ODE model.

For closed-loop simulations, setpoint tracking is performed for the average temperature in each cluster. Heat generation is restricted to two nodes per cluster, for a total of 12 input nodes. These nodes are specified by the enlarged nodes in Fig. 9, with $u_i = 0$ for the rest of the nodes.

7.1. Non-random ODE system generation by PCE

The ODE system (89) can be rewritten as the LTI system:

$$\frac{\mathrm{d}x}{\mathrm{d}t} = A(\theta_1)x + B(\theta_2)u, \tag{91}$$

where $x = [T_1, T_2, \dots, T_{118}]$, $u = [u_1, u_2, \dots, u_{118}]$, $A(\theta_1) = K_{\text{nom}}(1+\theta_1\Delta_1) - \eta_1 I_{118}$, and $B(\theta_2) = B_{\text{nom}}(1+\theta_2\Delta_2)$ for some nominal system matrices K_{nom} and B_{nom}. From (90), the entries of K_{nom} are given by

$$(K_{\text{nom}})_{ij} = \begin{cases} k_{\text{nom}}\dfrac{\bar{d}}{d_{ij}} & \text{if } j \in \mathcal{N}_i, \\ -\sum_{j\in\mathcal{N}_i} k_{\text{nom}}\dfrac{\bar{d}}{d_{ij}} & \text{if } i = j, \\ 0 & \text{otherwise,} \end{cases} \tag{92}$$

and $B_{\text{nom}} = \eta_{2,\text{nom}} I$.

For $\theta_1, \theta_2 \sim U([-1,1])$, similar to the previous case study, Table 1 indicates that Legendre polynomials are the appropriate PCE basis set to use. For this case study, a fourth-order expansion on the two random parameters, i.e, $d = 4$ and $n = 2$ in (43), is used to obtain

$$x = \sum_{\substack{i,j \\ i+j\le 4}} x_{i,j}\Phi_i(\theta_1)\Phi_j(\theta_2) = \sum_{k=1}^{15} x_k\phi_k(\theta), \tag{93}$$

where $\theta = [\theta_1, \theta_2]^\top$ and the variable k have been re-indexed for convenience in the stochastic Galerkin projection calculations later.

The expanded non-random ODE system for the PCE coefficients can be computed using the stochastic Galerkin projection method explicitly. Specifically, using the truncated PCE approximation as described in Section 4.1, the time evolution equation for each PCE coefficient is

$$\begin{aligned}\frac{\mathrm{d}x_j}{\mathrm{d}t} &= \left\langle \phi_j(\theta), \sum_{k=1}^{15} A(\theta)x_k\phi_k(\theta) + B(\theta)u \right\rangle \\ &= \sum_{k=1}^{15}\langle\phi_j(\theta)A(\theta)\phi_k(\theta)\rangle x_k + \langle B(\theta)\phi_j(\theta)\rangle u\ .\end{aligned}$$

Denote $\mathcal{X} = \text{vec}[x_1, x_2, \dots, x_{15}]$, $\mathcal{A}$ to be the PCE-expanded system matrix with block sub-matrices defined by $\mathcal{A}_{i,j} := (\langle\phi_j(\theta)A(\theta)\phi_k(\theta)\rangle)_{j,k}$, and similarly $\mathcal{B} := [\langle B(\theta)\phi_1(\theta)\rangle^\top, \langle B(\theta)\phi_2(\theta)\rangle^\top, \dots, \langle B(\theta)\phi_{15}(\theta)\rangle^\top]^\top$ to be the PCE-expanded input matrix. Then the time evolution of the PCE coefficients is described by the deterministic ODE

$$\frac{\mathrm{d}\mathcal{X}}{\mathrm{d}t} = \mathcal{A}\mathcal{X} + \mathcal{B}u\ . \tag{94}$$

An explicit closed form for the matrices $\mathcal{A}$ and $\mathcal{B}$ can further be obtained by observing that

$$\begin{aligned}\langle\phi_j(\theta)A(\theta)\phi_k(\theta)\rangle &= \langle\phi_j(\theta)\big(K_{\text{nom}}(1+\theta_1\Delta_1) - \eta_1 I\big)\phi_k(\theta)\rangle \\ &= \Big(\langle\phi_j(\theta)\phi_k(\theta)\rangle + \Delta_1\langle\theta_1\phi_j(\theta)\phi_k(\theta)\rangle\Big)K_{\text{nom}} \\ &\quad - \eta_1\delta_{ij}I \\ &= (\delta_{ij} + \Delta_1\langle\theta_1\phi_j(\theta)\phi_k(\theta)\rangle)K_{\text{nom}} - \eta_1\delta_{jk}I, \\ \langle B(\theta)\phi_j(\theta)\rangle &= \langle(1+\Delta_2\theta_2)\phi_j(\theta)\rangle B_{\text{nom}},\end{aligned}$$

which gives

$$\mathcal{A} = (I_{15} + \Delta_1 S)\otimes K_{\text{nom}} - \eta_1 I_{15}\otimes I_{118}\ , \tag{95}$$

$$\mathcal{B} = v\otimes B_{\text{nom}}\ , \tag{96}$$

where $S_{jk} := \langle\theta_1\phi_j(\theta)\phi_k(\theta)\rangle$ and $v_j = \langle(1+\Delta_2\theta_2)\phi_j(\theta)\rangle$.

7.2. Benchmarking forward uncertainty propagation with Monte Carlo sampling

To benchmark the accuracy of the PCE-approximated dynamics as in Section 6.2, Monte Carlo simulations are performed by solving the ODE system for various sample draws of $\theta_1, \theta_2 \sim U([-1,1])$. In each simulation run, the state was initially at the origin, and the control action used was $u_i = 1$ for all the nodes chosen for heat generation (2 nodes for each cluster, see Fig. 9) and $u_i = 0$ otherwise. In comparison, the solution of the expanded linear ODE system in (94) produces a time-varying set of PCE coefficients that induce an approximate probability distribution for the average temperatures of each cluster. These distributions can then

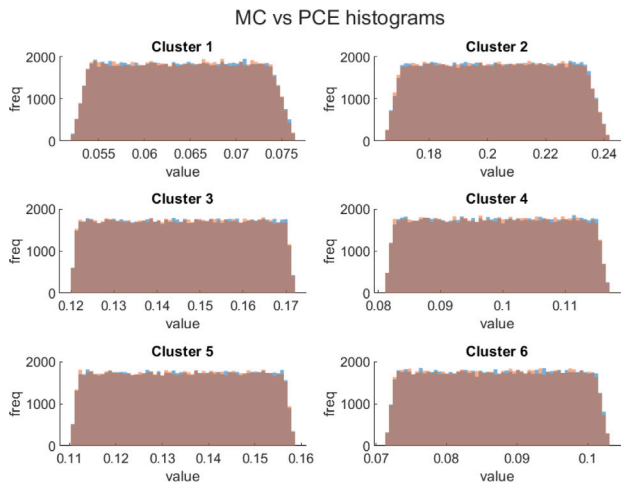

Fig. 10. Histograms for 100 000 random samples of each cluster average temperature at the final time $t = 5$ generated by Monte Carlo simulations (orange) and expanded PCE coefficient ODE system (blue). (For interpretation of the references to color in this figure legend, the reader is referred to the web version of this article.)

be approximated by sampling various values of $\{\theta_1, \theta_2\}$ and applying PCEs in the sense of Theorem 3 and (37).

Similar to the previous case study, the histograms for the cluster average temperatures using the Monte Carlo sampling-simulated distribution and the PCE-approximated distribution are compared in Fig. 10. The histograms show negligible differences in the shapes of the probability distribution, and the relative errors between the PCE-approximated variance and the Monte Carlo benchmarks are less than 0.13%. This demonstrates that PCE approximations have high numerical accuracy in quantifying output uncertainty, even for large-scale MIMO systems such as the IEEE 118-bus example.

7.3. Open-loop analysis problem: Input-output response disturbance-free system identification

Similar to the methodology used in Section 6.3, numerical time integration of the expanded ODE system for the PCE coefficients in (94) is performed by applying a unit step response $u = 1$ to each representative in Fig. 9, and observing the response of the PCE-expanded model until $t = 20$. Due to spatial constraints with the large number of control actions and nodes, the plots of the step responses are omitted, but are provided by the MATLAB scripts associated with this article. With the output responses measured, the PCE-based step-response matrices $\mathcal{G}_i^{\text{PCE}}$ given by (51) are computed by taking the response at every time interval of length 1.

7.4. Closed-loop synthesis problem: PCE-based QDMC performance

Similar to Section 6.4, the control action was computed using the formulation in (87) and (88) at each discrete sampling time t. All control parameters are provided in Table 5. The weight matrices and the output constraint are relatively large in size and are provided in the MATLAB code in the Github repository. The coefficient matrices $\mathcal{G}_i^{\text{PCE}}$ identified in the previous subsection are used for the predictive model $\hat{y}^{\text{PCE}}(t+i|t)$.

In order to evaluate the performance of the PCE-based QDMC strategy on this MIMO system, closed-loop simulations of the system are performed using a performance index for setpoint tracking of the various cluster average temperatures. Similar to Section 6.4, the setpoint is stepped up and down every 100 s, and the goal is to perform setpoint tracking for the desired cluster average temperatures. Fig. 11 plots the output responses for 100 random samples of θ_1 and θ_2. The closed-loop responses show that PCE-based QDMC is able to perform robust setpoint tracking for MIMO systems, even though the underlying state space is much larger for this case study.

Table 5
Controller parameters used in PCE-based QDMC closed-loop simulations for Section 7. Weight matrices $\mathcal{W}_y^{\text{PCE}}$ and W_u, and extended output constraint vectors $y_{\min}^{\text{PCE}}$ and $y_{\max}^{\text{PCE}}$, are all provided in the MATLAB files available at Github.

Controller parameter	Description	Nominal value	Units
Δt	Sampling time step	1	s
N	Model truncation number	20	–
p	Prediction horizon length	20	–
c	Control horizon length	5	–
$u_{\min}$	Minimum control action value	−100	–
$u_{\max}$	Maximum control action value	100	–
$\Delta u_{\min}$	Minimum control action decrease	−25	–
$\Delta u_{\max}$	Maximum control action increase	25	–
$y_{\min}$	Minimum cluster average temperature	−2	–
$y_{\max}$	Maximum cluster average temperature	2	–

To show that the PCE-based QDMC controller performs well in the presence of input and output disturbances for MIMO systems, an additional two separate closed-loop simulations are performed, one with moderate input disturbances of $d_u = \pm 10$ and one with moderate output disturbances of $d_y = \pm 0.5$. The results are shown in Fig. 12 for the input disturbances, and Fig. 13 for the output disturbances. Similar to the previous CSTR case study, the closed-loop trajectories all show that the PCE-based QDMC controller has good setpoint tracking properties for various realizations of the uncertain parameters, even in the presence of output and input disturbances.

8. Benchmarking various QDMC approaches

This section benchmarks the various QDMC approaches proposed in Section 5.2 and compares the quality of their output responses for both numerical case studies. We also include the controller formulation in Paulson et al. (2014) that is not offset-free.[8] This section adopts the nomenclature:

- **Strategy 1:** PCE-based QDMC with Output Measurement Variance of Zero;
- **Strategy 2:** Stochastic QDMC approach from Paulson et al. (2014);
- **Strategy 3:** PCE-based QDMC with Zero-variance Weight;
- **Strategy 4:** PCE-based QDMC with Variance Prediction Reset to Zero.

To avoid visual clutter, only the output trajectories are presented in the main discussion, while the control trajectories are given in Appendix. To quantitatively assess the performance and robustness of the various QDMC strategies, we report the average integral absolute error (IAE) and the width of the trajectory envelope for various realizations of parametric uncertainties. For the envelope width, the difference between the maximum output value and the minimum output value at the final time for various trajectories is used as a surrogate for how well the strategy responds to setpoint changes and input or output disturbances.

8.1. Comparison of closed-loop performance for case study 1

Fig. 14 compares the output trajectories for various realizations of parametric uncertainties k_1 and k_2 across the three disturbance scenarios: no disturbances (ND), input disturbances (ID), and output disturbances (OD). The control trajectories are shown in Fig. 17 in Appendix A.4. The strategies are quantitatively evaluated using the IAE

[8] That formulation is not offset-free, specifically because the output measurement and setpoint reference exclude higher order PCE coefficients.

Table 6
Closed-loop performance metrics for Case Study 1. The IAE and envelope width metrics are computed for three categories of disturbed systems, where "ND" stands for "no disturbance", "ID" stands for "input disturbance", and "OD" stands for "output disturbance". Metrics are averaged over multiple uncertainty realizations.

Strategy	IAE (ND)	Envelope width (ND)	IAE (ID)	Envelope width (ID)	IAE (OD)	Envelope width (OD)
1	0.129	8.44×10^{-9}	0.201	1.16×10^{-6}	0.278	3.37×10^{-6}
2	0.508	8.19×10^{-4}	0.551	8.19×10^{-4}	0.632	8.17×10^{-4}
3	0.0925	4.03×10^{-11}	0.125	4.36×10^{-11}	0.192	4.86×10^{-11}
4	0.0961	7.26×10^{-12}	0.137	1.837×10^{-10}	0.200	2.94×10^{-10}

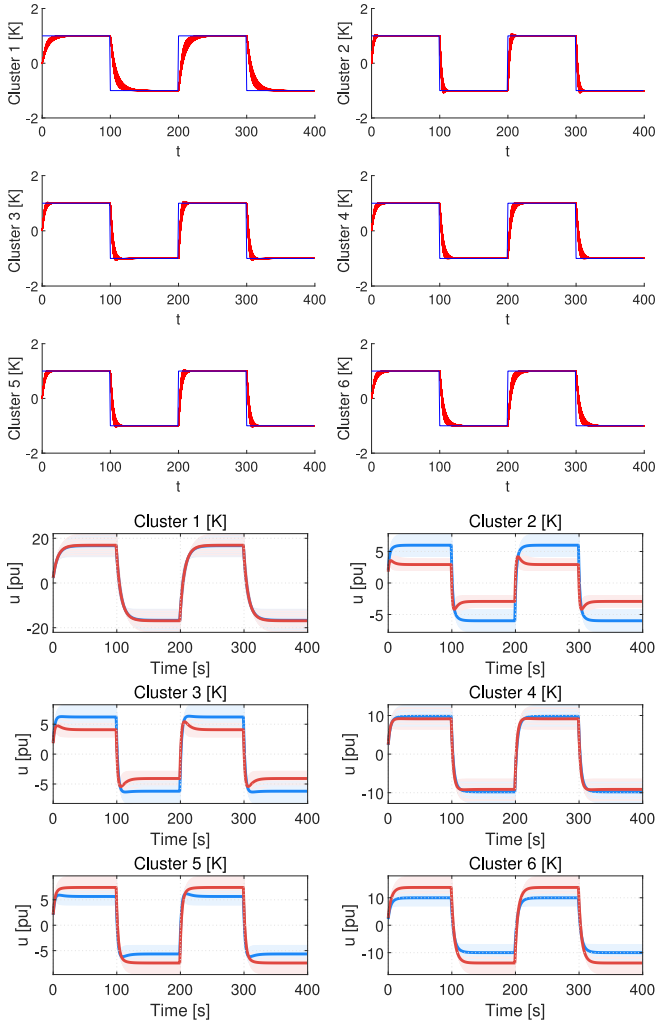

Fig. 11. Top three rows: Closed-loop output responses (red) for the cluster average temperatures for 100 realizations of the random parameters θ_1 and θ_2. All trajectories quickly reach the setpoint (blue) with effectively zero offset. Bottom three rows: Control trajectories for 100 realizations of the random parameters θ_1 and θ_2 for the two representative nodes from each cluster. Mean trajectories are shown by the solid red and blue lines. (For interpretation of the references to color in this figure legend, the reader is referred to the web version of this article.)

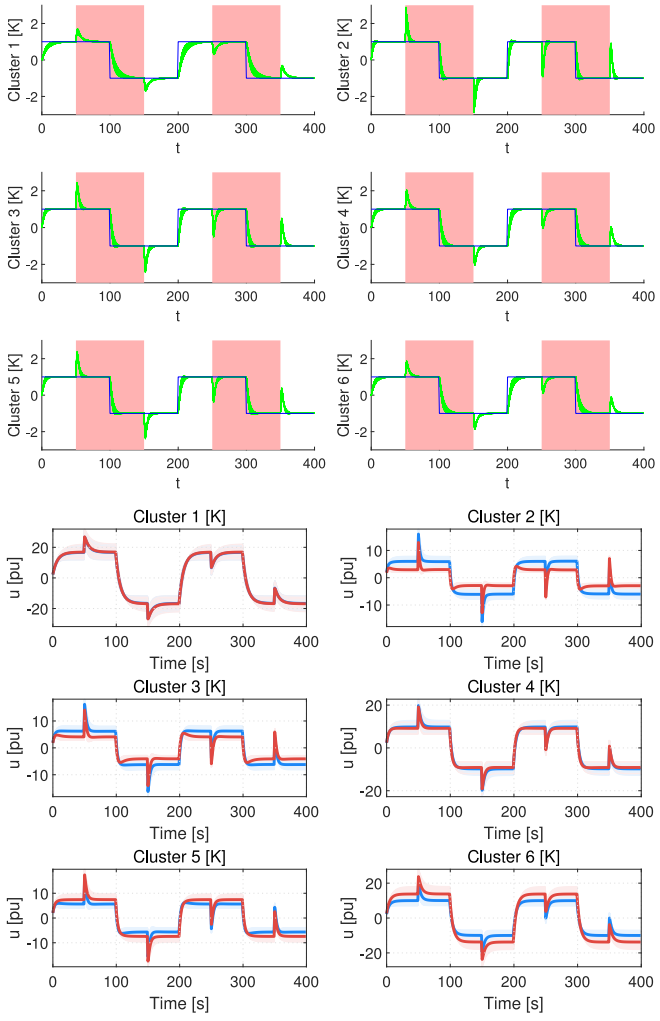

Fig. 12. Top three rows: Closed-loop responses (green) for the cluster average temperatures for 100 realizations of the random parameters θ_1 and θ_2, and two constant input disturbances (red): the first at $d_u = 0.5$ for $t \in [50, 150]$ s, and the second at $d_u = -0.5$ for $t \in [250, 350]$ s. Under several changes in the setpoint at times $t_{sp} \in \{100, 200, 300\}$ s, all trajectories quickly reach the setpoint (blue) with effectively zero offset. Bottom three rows: Control trajectories for 100 realizations of the random parameters θ_1 and θ_2 for the two representative nodes from each cluster. Mean trajectories are shown by the solid red and blue lines. (For interpretation of the references to color in this figure legend, the reader is referred to the web version of this article.)

and envelope width at the final time, where the metrics are averaged over all output trajectories and reported in Table 6.

In Case Study 1, Strategy 3 shows the best performance, with the lowest IAE and envelope width across various trajectories. Strategy 1, which is the strategy used in Sections 6 and 7, follows closely behind Strategy 3. Both of these strategies exhibit narrow closed-loop trajectory envelopes and fast setpoint tracking. Where the controller is not saturated, i.e., the ND and ID cases, the closed-loop responses eliminate offset for various realizations of the parametrically uncertain system. This is consistent with the fact that Strategies 1 and 3 are designed with integral action.

Strategy 4 also shows relatively good performance in the IAE and envelope width metrics, but there is much more overshoot, i.e., the controller action is more aggressive. Overshoot indicates underestimation of the variance terms, since all higher order PCE coefficients in the free

Table 7
Closed-loop performance metrics for Case Study 2. The IAE and envelope width metrics are computed for three categories of disturbed systems, where "ND" stands for "no disturbance", "ID" stands for "input disturbance", and "OD" stands for "output disturbance". Metrics are averaged over all clusters and multiple uncertainty realizations.

Strategy	IAE (ND)	Envelope width (ND)	IAE (ID)	Envelope width (ID)	IAE (OD)	Envelope width (OD)
1	25.55	2.29×10^{-5}	46.48	7.71×10^{-4}	34.94	8.55×10^{-4}
2	56.54	4.72×10^{-2}	74.85	4.76×10^{-2}	61.86	4.76×10^{-2}
3	102.80	5.40×10^{-2}	144.85	5.99×10^{-2}	119.76	7.75×10^{-2}
4	24.05	6.24×10^{-5}	43.61	2.18×10^{-3}	32.83	1.54×10^{-3}

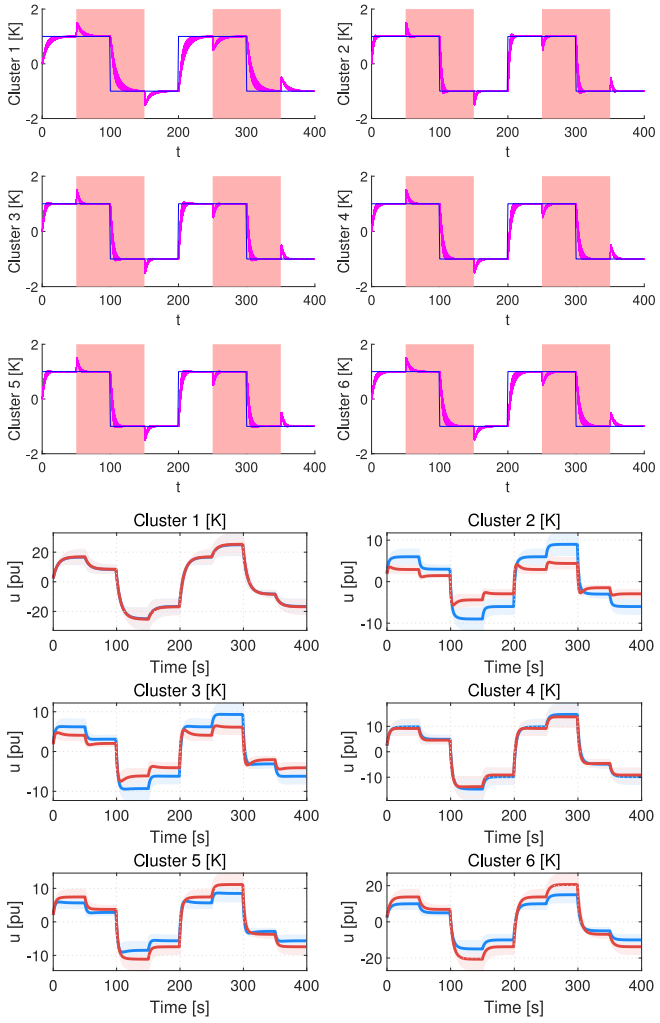

Fig. 13. Top three rows: Closed-loop responses (magenta) for the cluster average temperatures for 100 realizations of the random parameters θ_1 and θ_2, and two constant output disturbances (red): the first at $d_y = 0.5$ for $t \in [50, 150]$ s, and the second at $d_y = -0.5$ for $t \in [250, 350]$ s. Under several changes in the setpoint at times $t_{sp} \in \{100, 200, 300\}$ s, all trajectories quickly reach the setpoint (blue) with effectively zero offset. Bottom three rows: Control trajectories for 100 realizations of the random parameters θ_1 and θ_2 for the two representative nodes from each cluster. Mean trajectories are shown by the solid red and blue lines. (For interpretation of the references to color in this figure legend, the reader is referred to the web version of this article.)

response are set to zero. Despite the overshoot, Strategy 4 eliminates offset by design and is distributionally similar to Strategies 1 and 3.

In stark contrast, Strategy 2 shows the worst performance among the four strategies, with noticeable offset for all three disturbance cases and a distributionally wide spread for various parametric uncertainty realizations. In the ID and OD cases, the offset is visually larger than in the other strategies, which is made more obvious when quantified as a two- to five-fold increase in the IAE for all three disturbed cases in Table 6. These results are consistent with the lack of integral action in the design of Strategy 2. The simpler Case Study 1 strategy comparisons clearly illustrate and quantify the efficacy of our proposed PCE-QDMC approaches in eliminating offset in the presence of parametric uncertainties.

8.2. Comparison of closed-loop performance for case study 2

For the higher dimensional Case Study 2, we again compare the output trajectories for various realizations of parametric uncertainties in θ_1 and θ_2 across the same three disturbance scenarios (ND, ID, and OD). The results for Strategies 1 and 2 are given in Fig. 15, and for Strategies 3 and 4, the results are given in Fig. 16. The control trajectories are given in Appendix A.4, with Strategies 1 and 2 appearing in Fig. 18 and Strategies 3 and 4 appearing in Fig. 19. Due to the inherently slower dynamics of the process, the differences between the output trajectories across the various strategies become significantly more pronounced than in Case Study 1. The IAE and envelope width results are reported in Table 7.

When averaging over all output responses at the six clusters, Strategies 1 and 4 now outperform the other two control strategies in terms of having both low IAEs and low envelope widths across all three disturbance scenarios. Strategy 4 performs best in the IAE metric, whereas Strategy 1 performs best in the envelope width metric. Similarly to the previous case study, Strategy 2 shows a noticeable offset in all disturbance scenarios, with the offset becoming more pronounced in the presence of input disturbances and output disturbances.

In contrast to the previous case study, the output trajectory envelope for Strategy 3 visually performs much worse in setpoint tracking than for Strategy 1. This observation is confirmed by the three- to four-fold increases in the IAE metric across all disturbance scenarios. 100- to 1000-fold increases in the envelope width metric are also observed. Although Strategy 3 is designed with integral action, the settling time for the output response is much longer, especially for clusters 1 and 6. We attribute this sluggishness of the controller response to the slower dynamics of the process in Case Study 2 relative to Case Study 1. With Strategy 3, the penalty on the variance terms is completely neglected, which results in wider output response envelopes. This design choice reduces the robustness of the control strategy because it does not eliminate offset for all parametric uncertainty realizations. This robustness loss is not as apparent in the CSTR process with faster dynamics.

Furthermore, the output trajectory envelope for Strategy 4 exhibits larger and higher frequency overshoots for all three disturbance scenarios in contrast to Case Study 1. We attribute this aggressive control action to the slower dynamics of the process and the underestimation of the variance terms in Strategy 4. Despite this, steady-state offset is still rapidly eliminated and regulated, which overall demonstrates that Strategy 4 is a more performant and robust SMPC strategy in Case Study 2 compared to Strategies 2 and 3.

8.3. Summary of closed-loop strategies

Across both case studies, Strategy 1 emerges as the most consistent performer, achieving both low IAEs and envelope widths. It provides a good trade-off between settling time, robustness to parametric uncertainty, and offset regulation, which are key attributes in SMPC formulations. Strategy 2 performs the worst in both case studies, exhibiting persistent offset, large ensemble spread, and significantly higher IAE measures across all disturbance scenarios. The improvement with Strategy 1 from Strategy 2 highlights the importance of offset regulation in the control of parametrically uncertain systems. Strategy 3, which is also an offset-free formulation, performs comparably well in the CSTR case study where the dynamics are much faster and uncertainties are relatively small. However, when parametric uncertainties compound with slower process dynamics to produce higher output variances, the performance of the overly conservative Strategy 3 degrades as shown in the IEEE-118 bus case study. Strategy 4 is similar to Strategy 1 in its ability to eliminate steady-state offset, but care must be taken to manage the overshoot that arises from the more aggressive controller action.

9. Practical benefits, limitations, and guidelines

The preceding case studies show that our SMPC formulation using PCE-based QDMC removes steady-state offsets even in the presence of parametric uncertainty in the model. This section formalizes the practical implications and benefits of these findings, and also remarks on the limitations of our SMPC formulation. We also provide some guidelines for implementation that are important for efficient dynamic optimization in the SMPC controller.

9.1. Practical benefits

Offset-free tracking: As demonstrated in the preceding sections and the numerical case studies, our formulation enables the removal of steady-state offset even in the presence of parametric uncertainty. Our proposed method is particularly useful in applications where models inherently carry large parametric uncertainties, such as chemical reactor networks or biological systems. In these applications, the variance of the kinetic rate constants is often on the same order as the rate constant nominal values. The proposed method is further useful when the application is safety-critical and growing output variations cannot be tolerated, e.g., in the operation of a bioreactor to deliver a biotherapeutic product meeting a tight purity specification. In these settings, due to the size of the uncertainty, traditional robust control methods may not be able to synthesize a controller that is robustly stable for the entire uncertainty set. Our SMPC formulation enables direct control of higher-order PCE coefficients as outputs, which achieves robust performance without the need for excessive conservatism.

Spectrally accurate representation of uncertainty: In many cases, the PCE truncation error decays sub-exponentially with the PCE order, which enables a spectrally accurate representation of the variance in the model outputs. When the model parameters are analytic functions (e.g., linear functions) of the uncertain parameter, this sub-exponential rate of decay is provable and the potential impact of the higher order terms on the variance has been rigorously quantified (see, e.g., Theorem 8.1 of Field and Grigoriu (2004) and Trefethen (2019) for a detailed treatment). In our numerical case studies, we observe that modest expansion orders of $d = 3$ or $d = 4$ are sufficient to capture the variance in the output uncertainty with negligible error, as shown by the histograms in Figs. 4 and 10 where we compare open-loop responses of the PCE-expanded model with high-fidelity Monte Carlo simulations. The difference in output distributions is negligible, with a relative variance error of about 0.6% and 0.13%, respectively. This explains why, in practice, the truncated higher order PCE terms contribute minimally to the performance of PCE-based SMPC controllers. With smaller expansion orders, the PCE-based QDMC methods become more computationally tractable than sampling-based methods are on industrial controller microprocessors, where compute hardware resources are very limited.

Straightforward integration with existing software: The PCE-expanded models are deterministic models that can extend from modern off-the-shelf MPC tools without reformulation. For example, the SMPC dynamic optimization problem in (88) is a quadratic program that can be implemented with any conventional optimization package such as Gurobi and IPOPT. This avoids (i) the computational complexity arising from sampling-based methods, and (ii) intricate reformulations of existing MPC tools that are required for other SMPC formulations, e.g., the stochastic error tube approach (Arcari et al., 2023).

9.2. Limitations

Curse of Dimensionality: Most industrial applications employ process models with more than $n = 2$ uncertain parameters and very large input, state, and output dimensions (all larger than what was explored in this work), leading to computational intractability on industrial microprocessor controllers. As seen in (43), for a given expansion order d, the number of expansion terms needed is $\mathcal{O}(n^d)$, which grows combinatorially with the number of parameters. In practice, however, sub-exponential decay of the PCE coefficients for analytic models implies that the expansion order d required to reach a desired PCE coefficient accuracy is usually not large. Further dimensionality reduction is possible via sparse PCE methods, which removes PCE terms that do not contribute significantly to the PCE-based variance in the output distributions (see, e.g., Fagiano and Khammash (2012)). By using smaller expansion orders and sparse PCE methods, the impact from the curse of dimensionality on the application is lessened, with PCE-based methods continuing to outperform sampling-based methods for the same systems.

Time-varying parametric uncertainty: Our proposed SMPC formulation only deals with time-invariant parametric uncertainties. For time-varying parametric uncertainties such as multiplicative white noise, in principle, Karhunen–Loève expansions can be applied to describe the time-varying nature of these uncertainties (Kim & Braatz, 2013). Unfortunately, we observed in these cases that the required expansion order is very high because the uncertainty is drawn from an infinite-dimensional random field rather than a vector space. This leads to greater computational complexity in open-loop simulations of the PCE-expanded model and in the closed-loop dynamic optimization problem. Fortunately, parametric uncertainties in most manufacturing systems are time invariant or have time variations that are much slower than the closed-loop dynamics. For the latter, the uncertain parameters will be practically indistinguishable from time invariant during the response of the control system to a setpoint change or a sudden disturbance. As such, most process models would remain just as useful and computationally tractable with PCE-based QDMC by not modeling time variations in the model parameters.

9.3. Technical guidelines

PCE order: The PCE expansion order d is one of the most important design choices for our formulation. For systems where the model parameters are linear functions of the uncertainty, we observed that a modest expansion order of 2–3 is sufficient to reproduce output distributions; whereas for nonlinear dependencies, a higher expansion order of 3–4 may be required, as evidenced by the case studies shown above. A practical workflow would be to gradually increment the expansion order, benchmark the open-loop output distribution from the PCE-expanded model against a high-fidelity Monte-Carlo simulation, and then choose the minimal expansion order that achieves the desired

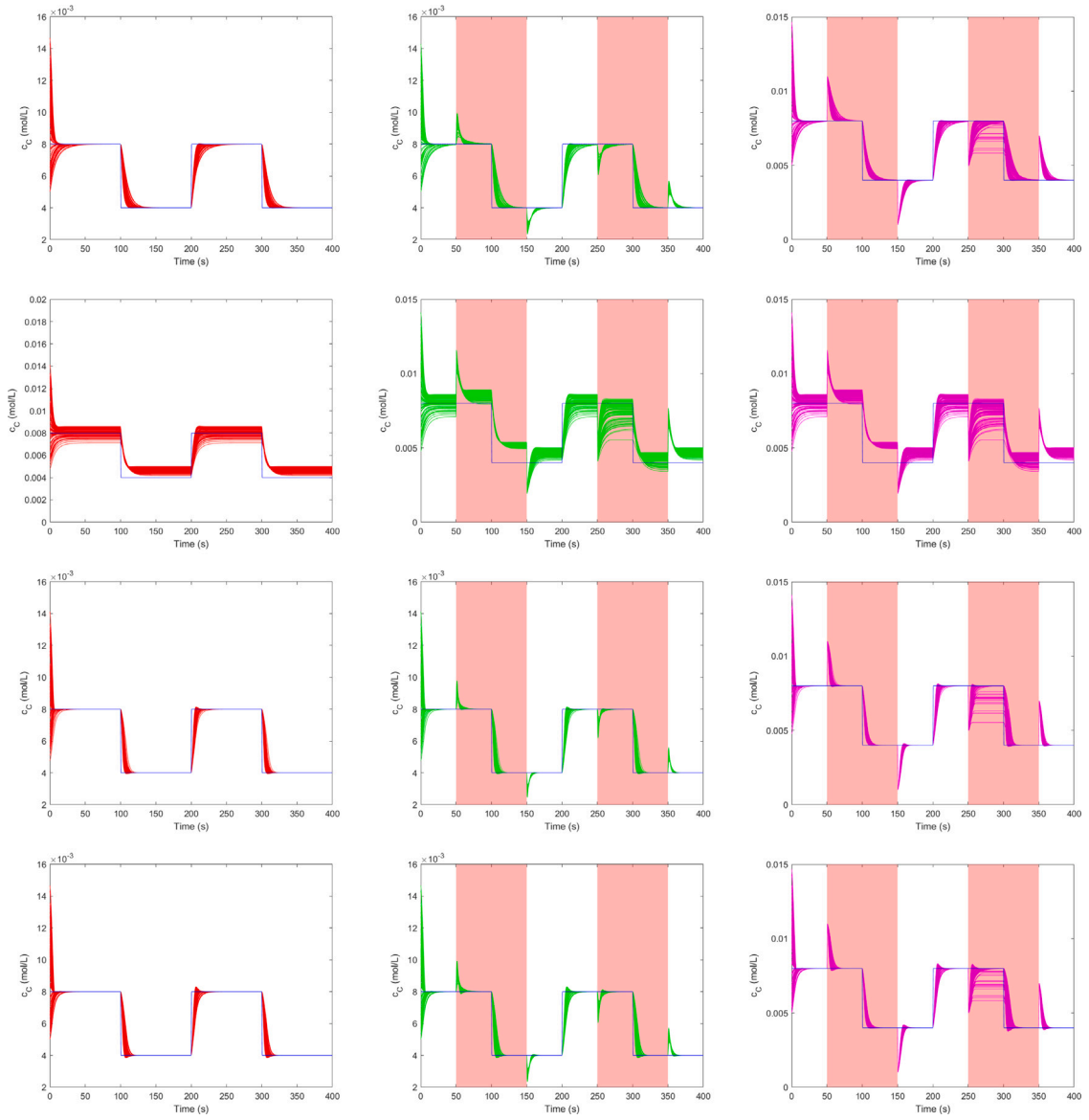

Fig. 14. Closed-loop output trajectories for Strategies 1–4 (rows) applied to Case Study 1, for the three disturbance cases as described in Section 6: no disturbances (left column; red), input disturbances (middle column; green), and output disturbances (right column; magenta). Each subplot shows responses for various parametric uncertainty realizations in tracking the setpoint (blue). The red shaded regions indicate periods when input or output disturbances are active, as detailed in the captions of Figs. 7 and 8. The corresponding input trajectories for these output trajectories are shown in Fig. 17. (For interpretation of the references to color in this figure legend, the reader is referred to the web version of this article.)

model accuracy. As seen in Figs. 4 and 10, when the output distributions are well-aligned, the PCE-expanded model can then be adopted for closed-loop controller formulation.

Warm-starting the optimizer: Because our SMPC controller formulation solves a quadratic program at every time step that could be large depending on the expansion order, a good initial guess for the optimal control trajectory in the control horizon is beneficial to reduce the computation time. The control actions in the previous optimal control profile can be index-shifted forward by one step and used to warm-start the optimizer for the problem at the current time. This strategy is also often used in deterministic MPC formulations (e.g., Rawlings et al. (2017)).

Sparse PCE: The computational cost can be greatly reduced for models in which the number of uncertain parameters is high by using sparse PCE (Lüthen, Marelli, & Sudret, 2021). Sparse PCE adaptively and optimally chooses the polynomial basis functions in (37) using specific metrics, such as degree adaptability (Blatman & Sudret, 2010). For large-scale systems with high-dimensional uncertainty, these sparse PCE methods can greatly reduce the dimensionality of the PCE-expanded model. We intend to explore sparse PCEs for SMPC formulations in future work.

Undersized Actuators: A large proportion of practical control problems have constraints that are only active transiently during large disturbances or setpoint changes. In such control problems, once the constraints are no longer active, the closed-loop system operates as an unconstrained system. Integral action is included in the control system so that the steady-state error approaches zero when the constraints are no longer active. This work considers this practically important use case.

For systems in which the actuators are undersized, it is not possible for the desired setpoint to be achieved for unconstrained values for the actuators under steady-state operations (see, e.g., Fig. 8). For such systems with undersized actuators, there is no reason to carry out analysis of whether there is zero steady-state error under those conditions, as it is not possible to achieve zero steady-state error for such systems.

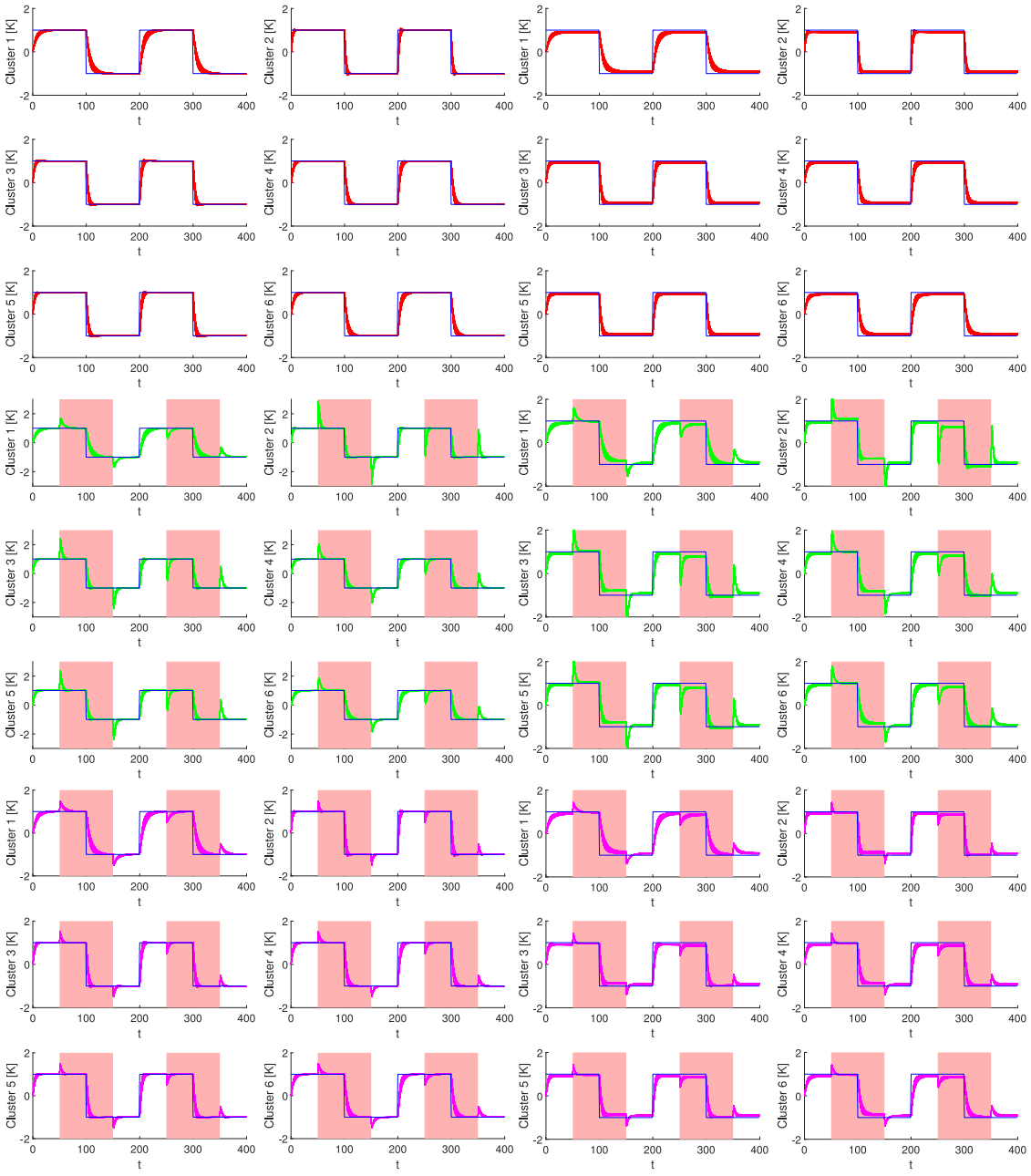

Fig. 15. Closed-loop output trajectories for Strategies 1 (left two columns) and 2 (right two columns) applied to Case Study 2, for the three disturbance cases as described in Section 7: no disturbances (top three rows; red), input disturbances (middle three rows; green), and output disturbances (bottom three rows; magenta). Each subplot shows responses for various parametric uncertainty realizations in tracking the setpoint (blue). The red shaded regions indicate periods when input or output disturbances are active, as detailed in the captions of Figs. 12 and 13. The corresponding input trajectories for these cluster average output trajectories are shown in Fig. 18. (For interpretation of the references to color in this figure legend, the reader is referred to the web version of this article.)

The proofs in this work show that a suite of PCE-based QDMC formulations have zero offset for operations in which the actuators are not required to be active at steady-state conditions. In the case studies, the optimal control actions obtained from QDMC were within the constraint limits at steady-state operations, so offset-free control was achieved except in Fig. 8.

10. Conclusion

This article describes PCE-based QDMC formulations for MIMO LTI process models that handle step changes in setpoints. Under mild assumptions, these controllers are proved to have single, full column-rank integrators which provide offset-free control for multiple performance indices simultaneously during step changes in the setpoints. The PCE-based controllers are applied to the control of the continuous synthesis of a high-value product in a nonlinear series–parallel reaction network. The PCE-based QDMC performs rapid and robust setpoint tracking—even in the presence of both (multiplicative) parametric uncertainty, and (additive) input and output disturbances. These QDMC formulations fulfill the offset-free performance objectives of continuously operated processes where the dynamics are approximated well as MIMO LTI responses with BIBO stability, and the setpoint changes are steps.

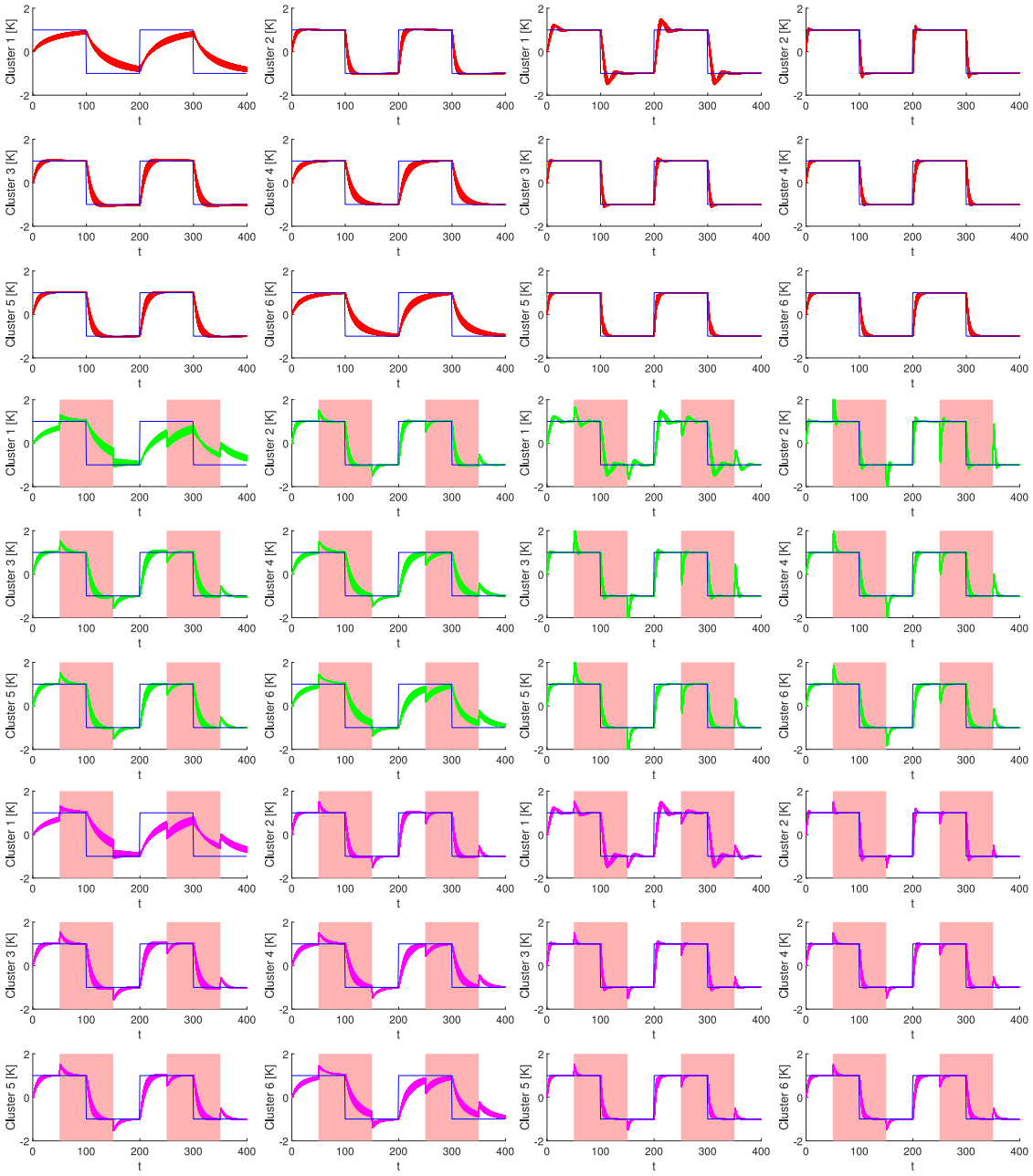

Fig. 16. Closed-loop output trajectories for Strategies 3 (left two columns) and 4 (right two columns) applied to Case Study 2, for the three disturbance cases as described in Section 7: no disturbances (top three rows; red), input disturbances (middle three rows; green), and output disturbances (bottom three rows; magenta). Each subplot shows responses for various parametric uncertainty realizations in tracking the setpoint (blue). The red shaded regions indicate periods when input or output disturbances are active, as detailed in the captions of Figs. 12 and 13. The corresponding input trajectories for these cluster average output trajectories are shown in Fig. 19. (For interpretation of the references to color in this figure legend, the reader is referred to the web version of this article.)

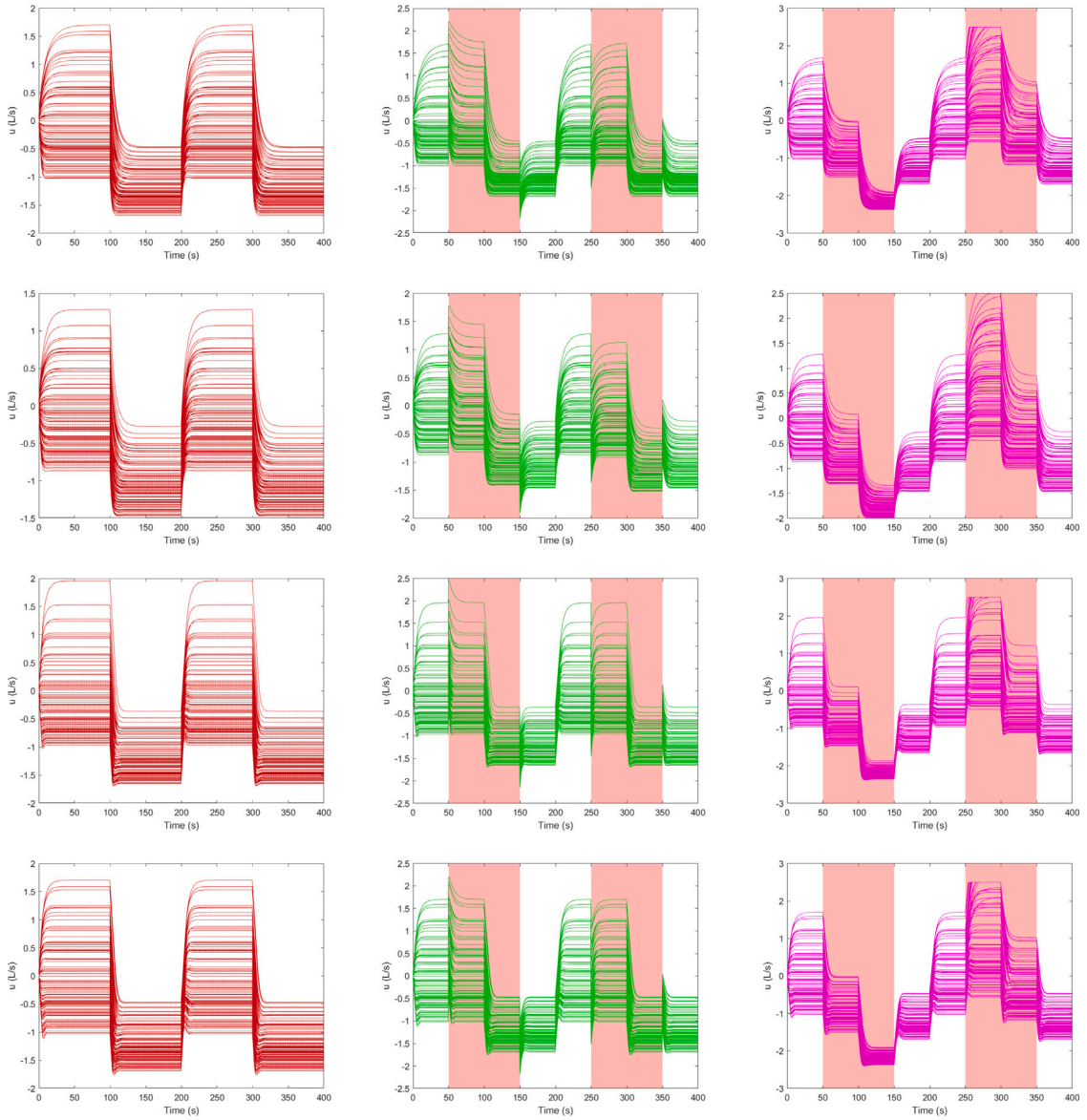

Fig. 17. Control trajectories for Strategies 1–4 (rows) applied to Case Study 1, for the three disturbance cases as described in Section 6: no disturbances (left column), input disturbances (middle column), and output disturbances (right column). Each subplot shows output responses for various parametric uncertainty realizations. The red shaded regions indicate periods when input or output disturbances are active, as detailed in the captions of Figs. 7 and 8. The corresponding output trajectories for these input trajectories are shown in Fig. 14. (For interpretation of the references to color in this figure legend, the reader is referred to the web version of this article.)

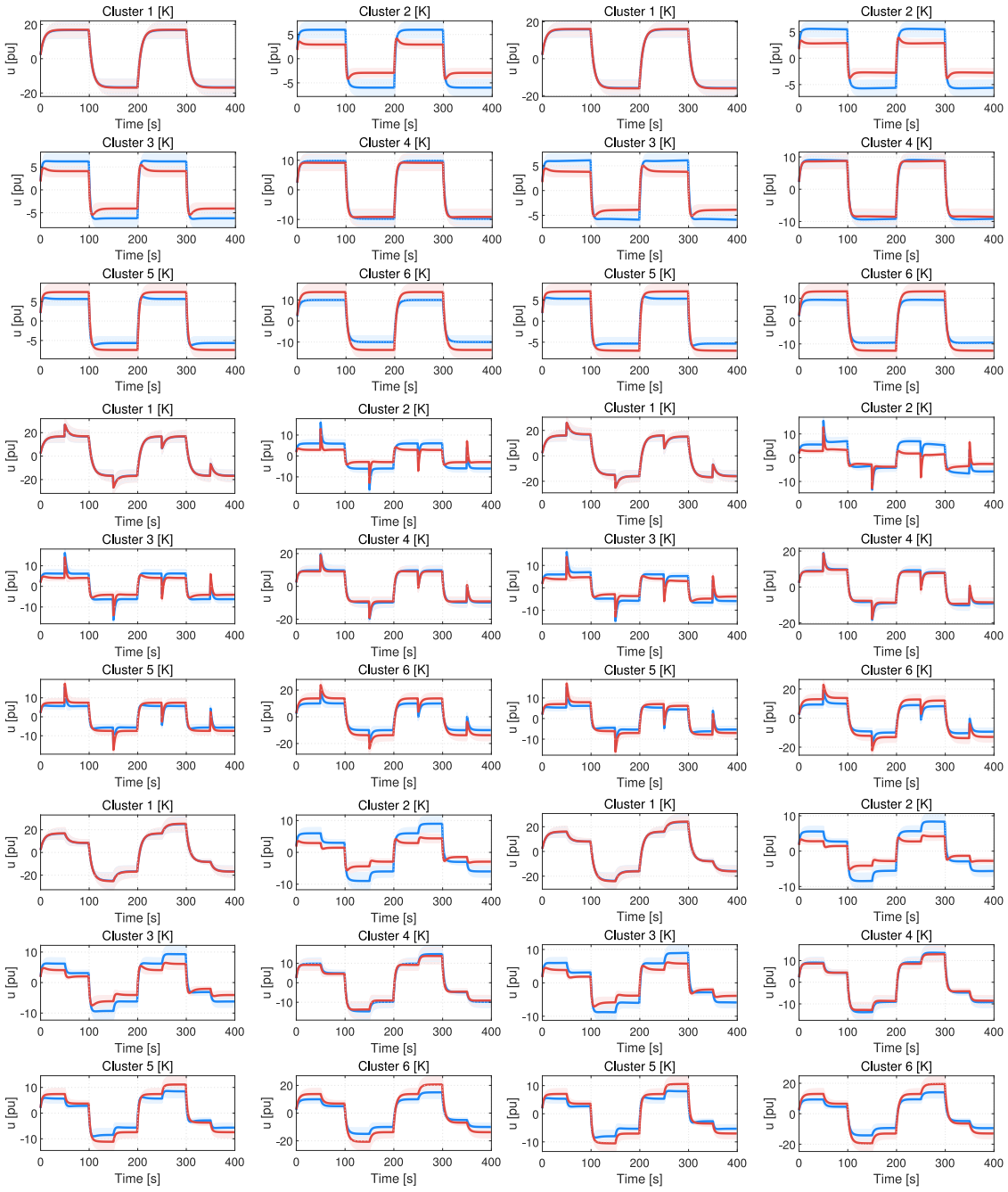

Fig. 18. Control trajectories for Strategies 1 (left two columns) and 2 (right two columns) applied to Case Study 2, for the three disturbance cases as described in Section 7: no disturbances (top three rows), input disturbances (middle three rows), and output disturbances (bottom three rows). Each subplot shows the mean trajectories for various parametric uncertainty realizations for the two representative nodes from each cluster (solid red and blue lines). The corresponding cluster average output trajectories for these input trajectories are shown in Fig. 15. (For interpretation of the references to color in this figure legend, the reader is referred to the web version of this article.)

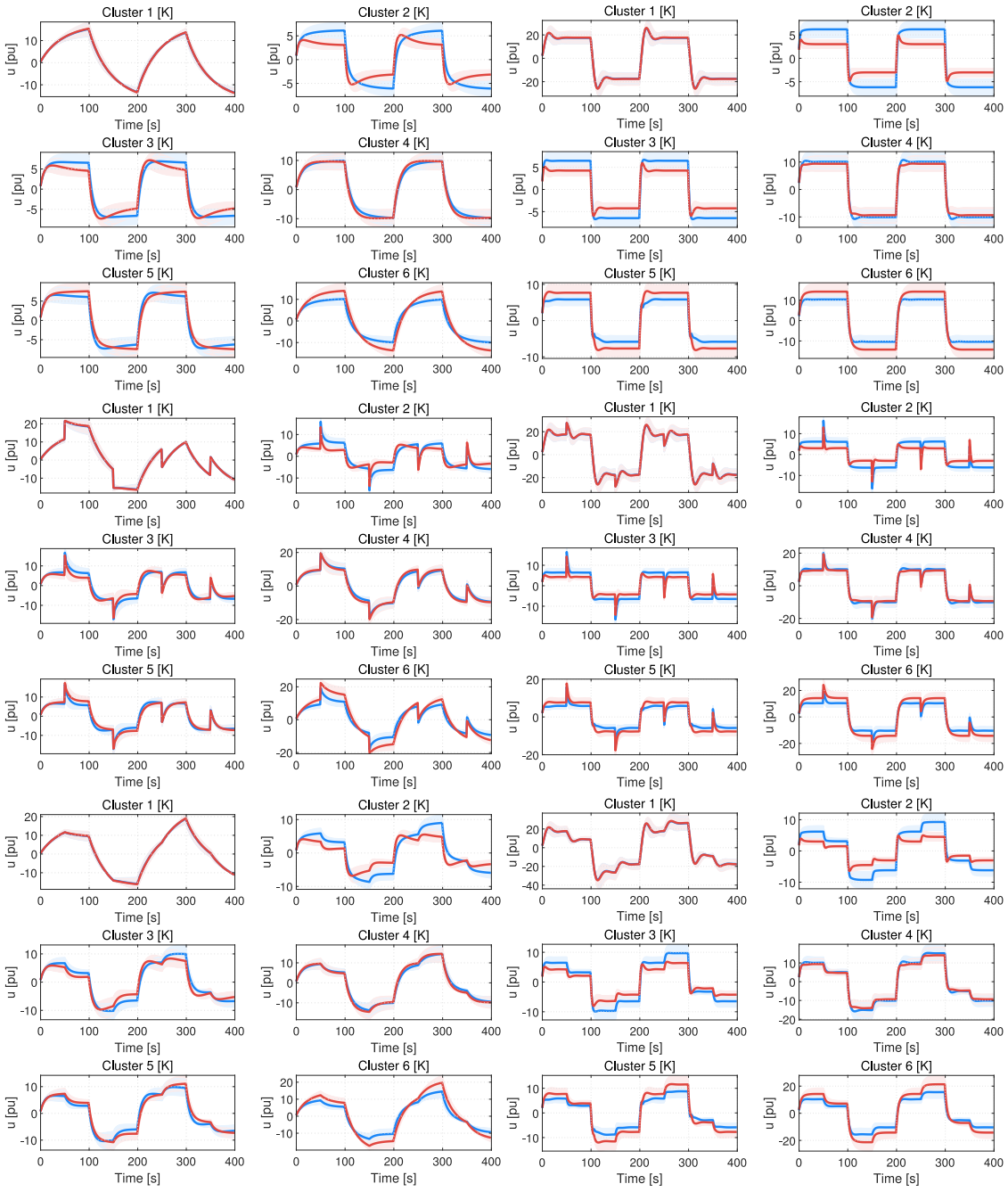

Fig. 19. Control trajectories for Strategies 3 (left two columns) and 4 (right two columns) applied to Case Study 2, for the three disturbance cases as described in Section 7: no disturbances (top three rows), input disturbances (middle three rows), and output disturbances (bottom three rows). Each subplot shows the mean trajectories for various parametric uncertainty realizations for the two representative nodes from each cluster (solid red and blue lines). The corresponding cluster average output trajectories for these input trajectories are shown in Fig. 16. (For interpretation of the references to color in this figure legend, the reader is referred to the web version of this article.)

CRediT authorship contribution statement

Wallace Gian Yion Tan: Writing – original draft, Validation, Software, Investigation, Formal analysis, Conceptualization. **Krystian Ganko:** Writing – original draft, Validation, Software, Investigation, Conceptualization. **Srimanta Santra:** Writing – review & editing, Supervision. **Matthias von Andrian:** Software, Methodology, Investigation, Formal analysis, Conceptualization. **Richard D. Braatz:** Writing – review & editing, Supervision, Project administration, Funding acquisition, Conceptualization.

Availability of code

All the code used to perform the various simulations and generate the figures in this manuscript may be found at https://github.com/wallytgy/PCE_QDMC.

Disclaimer

This report was prepared as an account of work sponsored by an agency of the United States Government. Neither the United States Government nor any agency thereof, nor any of their employees, makes

Declaration of competing interest

The authors declare that they have no known competing financial interests or personal relationships that could have appeared to influence the work reported in this paper.

Acknowledgments

Financial support is acknowledged by Contract 75F40122C00200 from the U.S. Food and Drug Administration. Krystian Ganko was primarily supported by the U.S. Department of Energy, Office of Science, Office of Advanced Scientific Computing Research, Department of Energy Computational Science Graduate Fellowship under Award Number DE-SC0022158. The authors would also like to thank Dr. Liang Wu, Dr. Yingjie Ma, and Maik Pfefferkorn for input and discussion regarding MPC formulations, most recent SMPC developments, and practical applications.

Appendix

The following proofs and additional references are provided to help formalize the context and significance of integrator action in the controller syntheses described in this work. The proofs are matched to their labeled lemma statements provided in Section 2.4 of the main text.

A.1. BIBO stability

Proof. Since all poles of $G(z)$ lie within the unit circle, $G(z)$ can be written in the form

$$G(z) = \sum_{i,j} \frac{1}{(z - z_i)^j} A_{i,j} + P(z), \tag{97}$$

where, for each ordered pair (i, j), the z_i pole has $|z_i| < 1$ and falls into a multiplicity class of size j; $A_{i,j} \in \mathbb{C}^{m\times n}$ is a constant matrix; and $P(z) \in \mathbb{C}^{m\times n}$ is a matrix with polynomial entries. $\mathcal{Z}^{-1}(P(z)U(z))$ is a bounded sequence, since it consists of linear combinations of time shifts of $u(t)$. Since $A_{i,j}$ is a constant matrix, it suffices to show that $\mathcal{Z}^{-1}\left((z - z_i)^{-j}U(z)\right)$ is bounded. For $z_i \neq 0$, this boundedness can be seen from

$$\mathcal{Z}^{-1}\left(\frac{1}{(z - z_i)^j}\right) = p_j(t)\mathbb{1}_{\{t\geq 1\}} z_i^{-j+t} =: h_{i,j}(t), \tag{98}$$

where p_j is a polynomial of degree j and $\mathbb{1}_{\{t\geq 1\}}$ is the indicator function for the set $\{t \mid t \geq 1\}$. For $z_i = 0$, then $\mathcal{Z}^{-1}\left((z - z_i)^{-j}U(z)\right) = \mathcal{Z}^{-1}\left((z)^{-j}U(z)\right)$ is a shift of the original sequence $U(z)$, which is bounded. Therefore, we see that $|h_{i,j}(t)| \leq C_{i,j}(|z_i| + \epsilon)^t$ for some $\epsilon > 0$ small enough and $C_{i,j} > 0$ depending on ϵ. Since multiplication in the Z-transform space is equivalent to convolution in the time domain, assuming that $u(t) \leq M$ where $M \in \mathbb{R}^n$ for all t, application of the Cauchy–Schwartz inequality implies that

$$\begin{aligned}\left\|\mathcal{Z}^{-1}\left((z - z_i)^{-j}U(z)\right)(t)\right\| &= \left\|\sum_{k=1}^{t} h_{i,j}(k)u(t-k)\right\| \\ &\leq M\sum_{k=0}^{t} |h_{i,j}(k)| \\ &\leq M\sum_{k=0}^{t} C_{i,j}(|z_i| + \epsilon)^k \\ &\leq MC_{i,j}(1 - |z_i| - \epsilon)^{-1}.\end{aligned} \tag{99}$$

This statement shows that $\mathcal{Z}^{-1}\left((z - z_i)^{-j}U(z)\right)$ is a bounded function of t. Since the sum of finitely many bounded sequences is bounded, $y(t) = \mathcal{Z}^{-1}(G(s)U(s))$ is also bounded. The inequality for $g(t)$ in the second part of the lemma readily follows from the inequality $|h_{i,j}(t)| \leq C_{i,j}(|z_i| + \epsilon)^t$ and by taking the maximum value of all such $|h_{i,j}(t)|$. □

For additional proofs of BIBO stability for general input–output systems, the reader is referred to, e.g., Desoer and Vidyasagar (1975). For a more practical treatment, the reader is referred to, e.g., Ogunnaike and Ray (1994).

A.2. Integrator action

Proof. As motivated by Lemma 1, express $K(z)$ using partial fractions to show that

$$K(z) = \frac{1}{z-1}K_{\mathrm{I}} + \tilde{K} = \frac{1}{z-1}K_{\mathrm{I}} + \sum_{i,j}\frac{1}{(z - z_i)^j}A_{i,j} + P(z). \tag{100}$$

Further, $d(t) := \mathcal{Z}^{-1}(\tilde{K}(z)E(z))$ is a bounded sequence by Lemma 1, so it suffices to show that

$$\mathcal{Z}^{-1}\left(K_{\mathrm{I}}(z-1)^{-1}U(z)\right) = K_{\mathrm{I}}\sum_{i=0}^{t} e(i), \tag{101}$$

which can be shown by directly calculating the inverse transform of $(z-1)^{-1}$ and then using the fact that convolution in the time domain is equivalent to multiplication in the Z-transform space. □

Rigorous proofs for both continuous- and discrete-time system integrators may be found in, e.g., Morari and Zafiriou (1989). Extensive discussion on the design and application of single and double integrators in sampled-data systems may be found in, e.g., Åström and Wittenmark (1984).

A.3. Multiple performance index closed-loop integrator action is offset-free

Proof. Define $d(t) := y_{\mathrm{sp}}(t) - c$, which implies that $\lim_{t\to\infty} d(t) = 0$. Taking the Z-transform of the setpoint and performing partial fraction decomposition results in

$$D(z) = Y_{\mathrm{sp}}(z) - \frac{c}{1 - z^{-1}} = Y_{\mathrm{sp}}(z) - \left(c + \frac{c}{z-1}\right). \tag{102}$$

The conditions and the statements proving Lemma 1 imply that the plant transfer function is

$$G(z) = (z-1)^k\tilde{G}(z) = (z-1)^k\left(\sum_{i,j}\frac{1}{(z - z_i)^j}A_{i,j} + P(z)\right), \tag{103}$$

where

$$\tilde{G}(z) := \sum_{i,j}\frac{1}{(z - z_i)^j}A_{i,j} + P(z). \tag{104}$$

By substitution of (102) and (103), the output error $E(z)$ may be expressed as

$$\begin{aligned}E(z) &= G(z)Y_{\mathrm{sp}}(z) \\ &= \left(\sum_{i,j}\frac{1}{(z - z_i)^j}A_{i,j} + P(z)\right)\Big(\, c(z-1)^k + c(z-1)^{k-1} \\ &\quad + (z-1)^k D(z)\,\Big).\end{aligned} \tag{105}$$

We next show that, for any sequence $x(t)$ such that $\lim_{t\to\infty} x(t) = 0$, $h(t) := \mathcal{Z}^{-1}(\tilde{G}(z)X(z))$ satisfies $\lim_{t\to\infty} h(t) = 0$. Then, since the inverse Z-transform of each of the three terms $c(z-1)^k$, $c(z-1)^{k-1}$, $(z-1)^k D(z)$ converges to zero as $t \to \infty$ (i.e., these terms are linear combinations of time-shifted sequences that converge to zero as $t \to \infty$), the error vector $e(t) = \mathcal{Z}^{-1}(G(z)Y_{\text{sp}}(z))$ also converges to the zero vector as $t \to \infty$.

Inequality (99) in Lemma 1 gives that $\|\tilde{g}(t)\|_2 \le C_g\left((\max_i |z_i| + \epsilon)^t\right)$ for every $\epsilon > 0$ and some $C_g > 0$ depending on ϵ. Let $\tilde{\epsilon} > 0$ be an arbitrary positive real number and define $r := \max_i |z_i| + \epsilon < 1$. We choose t_0 large enough such that $\|\tilde{g}(t)\|_2 < \tilde{\epsilon}$ and $x(t) \le \tilde{\epsilon}$ for all $t \ge \lfloor t_0/2 \rfloor$. Then, assuming $\left\|y_{\text{sp}}(t)\right\| < M$ and $t \ge t_0$,

$$\begin{aligned}\|h(t)\| &= \left\|\sum_{q=0}^{t} \tilde{g}(q)x(t-q)\right\| \\ &\le \left\|\sum_{q=0}^{\lfloor t/2 \rfloor} \tilde{g}(q)x(t-q)\right\| + \left\|\sum_{q=\lfloor t/2 \rfloor}^{t} \tilde{g}(q)x(t-q)\right\| \\ &\le \frac{\tilde{\epsilon}}{1-r} + \frac{M\tilde{\epsilon}r^{\lfloor t/2 \rfloor}}{1-r}.\end{aligned}$$

Since $\tilde{\epsilon}$ is an arbitrary positive real number, the proof is complete. □

We again make reference to Morari and Zafiriou (1989) for proofs and discussion on offset-free integrator action in MIMO systems.

A.4. Control trajectories for Section 8

Control trajectories for Case Study 1 are shown in Fig. 17, and control trajectories for Case Study 2 are shown in Figs. 18 and 19.

References

Åström, K. J., & Wittenmark, B. (1984). *Computer controlled systems: Theory and design*. Englewood Cliffs, NJ: Prentice Hall.

Arcari, E., Iannelli, A., Carron, A., & Zeilinger, M. N. (2023). Stochastic MPC with robustness to bounded parameteric uncertainty. *IEEE Transactions on Automatic Control*, *68*(12), 7601–7615.

Bemporad, A., Puglia, L., & Gabbriellini, T. (2011). A stochastic model predictive control approach to dynamic option hedging with transaction costs. In *American control conference* (pp. 3862–3867).

Blatman, G., & Sudret, B. (2010). An adaptive algorithm to build up sparse polynomial chaos expansions for stochastic finite element analysis. *Probabilistic Engineering Mechanics*, *25*(2), 183–197.

Boyd, J. P. (2001). Chebyshev and fourier spectral methods, *Dover books on mathematics*, (2nd ed.). Mineola, NY: Dover Publications.

Brewer, J. W. (1978). Kronecker products and matrix calculus in system theory. *IEEE Transactions on Circuits and Systems*, *25*(9), 772–781.

Cameron, R. H., & Martin, W. T. (1947). The orthogonal development of non-linear functionals in series of Fourier-Hermite functionals. *Annals of Mathematics*, 385–392.

Chen, C.-T. (1984). Linear system theory and design. *HRW series in electrical and computer engineering*, Orlando, FL: Holt, Rinehart and Winston.

Couaillier, V., & Savin, É. (2019). Generalized polynomial chaos for non-intrusive uncertainty quantification in computational fluid dynamics. In C. Hirsch, D. Wunsch, J. Szumbarski, L. Łaniewski-Wołłk, & J. Pons-Prats (Eds.), *Notes on numerical fluid mechanics and multidisciplinary design*, *Uncertainty management for robust industrial design in aeronautics* (pp. 123–141). Cham, Switzerland: Springer.

Cutler, C. R., & Ramaker, B. L. (1980). Dynamic matrix control—A computer control algorithm. In *17th joint automatic control conference* (pp. 1–6). Paper WP5-B.

Davis, P. J., & Polonsky, I. (1972). Numerical interpolation, differentiation, and integration. In M. Abramowitz, & I. A. Stegun (Eds.), *Handbook of mathematical functions with formulas, graphs, and mathematical tables* (10th ed.). (pp. 875–899). Washington, DC: United States Government Printing Office.

Davis, P. J., & Rabinowitz, P. (1984). Methods of numerical integration, *Computer science and applied mathematics*, (2nd ed.). San Diego, CA: Academic Press.

Desoer, C. A., & Vidyasagar, M. (1975). *Feedback systems: Input-output properties*. New York, NY: Academic Press.

Ernst, O. G., Mugler, A., Starkloff, H.-J., & Ullmann, E. (2012). On the convergence of generalized polynomial chaos expansions. *ESAIM. Mathematical Modelling and Numerical Analysis*, *46*(2), 317–339.

Fagiano, L., & Khammash, M. (2012). Nonlinear stochastic model predictive control via regularized polynomial chaos expansions. In *51st IEEE conference on decision and control* (pp. 142–147).

Fagiano, L., Schildbach, G., Tanaskovic, M., & Morari, M. (2015). Scenario and adaptive model predictive control of uncertain systems. *IFAC-PapersOnLine*, *48*(23), 352–359.

Field, R. V., Jr., & Grigoriu, M. (2004). On the accuracy of the polynomial chaos approximation. *Probabilistic Engineering Mechanics*, *19*(1–2), 65–80.

Filip, S., Javeed, A., & Trefethen, L. N. (2019). Smooth random functions, random ODEs, and Gaussian processes. *SIAM Review*, *61*(1), 185–205.

Finn, C. K., Wahlberg, B., & Ydstie, B. E. (1993). Constrained predictive control using orthogonal expansions. *AIChE Journal*, *39*(11), 1810–1826.

Garcia, C. E., & Morshedi, A. (1986). Quadratic programming solution of dynamic matrix control (QDMC). *Chemical Engineering Communications*, *46*(1–3), 73–87.

Heirung, T. A. N., Paulson, J. A., O'Leary, J., & Mesbah, A. (2018). Stochastic model predictive control—How does it work? *Computers & Chemical Engineering*, *114*, 158–170.

Hsu, S.-C., & Bhattacharya, R. (2020). Design of linear parameter varying quadratic regulator in polynomial chaos framework. *International Journal of Robust and Nonlinear Control*, *30*(16), 6661–6682.

Kim, K.-K. K., & Braatz, R. D. (2012). Generalized polynomial chaos expansion approaches to approximate stochastic receding horizon control with applications to probabilistic collision checking and avoidance. In *IEEE international conference on control applications* (pp. 350–355).

Kim, K.-K. K., & Braatz, R. D. (2013). Generalised polynomial chaos expansion approaches to approximate stochastic model predictive control. *International Journal of Control*, *86*(8), 1324–1337.

Kim, K.-K. K., Shen, D. E., Nagy, Z. K., & Braatz, R. D. (2013). Wiener's polynomial chaos for the analysis and control of nonlinear dynamical systems with probabilistic uncertainties. *IEEE Control Systems*, *33*(5), 58–67.

Ljung, L. (1999). System identification: Theory for the user, *Prentice hall information and system sciences series*, (2nd ed.). Upper Saddle River, NJ: Prentice Hall PTR.

Lucia, S., Zometa, P., Kögel, M., & Findeisen, R. (2015). Efficient stochastic model predictive control based on polynomial chaos expansions for embedded applications. In *54th IEEE conference on decision and control* (pp. 3006–3012).

Lucor, D., Su, C.-H., & Karniadakis, G. E. (2004). Generalized polynomial chaos and random oscillators. *International Journal for Numerical Methods in Engineering*, *60*(3), 571–596.

Lundström, P., Lee, J. H., Morari, M., & Skogestad, S. (1995). Limitations of dynamic matrix control. *Computers & Chemical Engineering*, *19*(4), 409–421.

Luo, W. (2006). *Wiener chaos expansion and numerical solutions of stochastic partial differential equations* (Ph.D. dissertation), Pasadena, CA: Department of Computing and Mathematical Sciences, California Institute of Technology.

Lüthen, N., Marelli, S., & Sudret, B. (2021). Sparse polynomial chaos expansions: Literature survey and benchmark. *SIAM/ASA Journal on Uncertainty Quantification*, *9*(2), 593–649.

Luyben, W. L. (2007). *Chemical reactor design and control*. Hoboken, NJ: John Wiley & Sons.

Maeder, U., Borrelli, F., & Morari, M. (2009). Linear offset-free model predictive control. *Automatica*, *45*(10), 2214–2222.

Maeder, U., & Morari, M. (2010). Offset-free reference tracking with model predictive control. *Automatica*, *46*(9), 1469–1476.

Mammarella, M., Lorenzen, M., Capello, E., Park, H., Dabbene, F., Guglieri, G., et al. (2018). An offline-sampling SMPC framework with application to autonomous space maneuvers. *IEEE Transactions on Control Systems Technology*, *28*(2), 388–402.

Mesbah, A. (2016). Stochastic model predictive control: An overview and perspectives for future research. *IEEE Control Systems Magazine*, *36*(6), 30–44.

Morari, M., & Lee, J. H. (1999). Model predictive control: Past, present and future. *Computers & Chemical Engineering*, *23*(4–5), 667–682.

Morari, M., & Zafiriou, E. (1989). *Robust process control*. Englewood Cliffs, NJ: Prentice Hall.

Muske, K. R., & Badgwell, T. A. (2002). Disturbance modeling for offset-free linear model predictive control. *Journal of Process Control*, *12*(5), 617–632.

Nocedal, J., & Wright, S. J. (2006). Numerical optimization, *Springer series in operations research and financial engineering*, (2nd ed.). New York: Springer.

Ogunnaike, B. A., & Ray, W. H. (1994). Process dynamics, modeling, and control. *Topics in chemical engineering*, New York: Oxford University Press.

Pannocchia, G., & Rawlings, J. B. (2003). Disturbance models for offset-free model-predictive control. *AIChE Journal*, *49*(2), 426–437.

Paulson, J. A., Mesbah, A., Streif, S., Findeisen, R., & Braatz, R. D. (2014). Fast stochastic model predictive control of high-dimensional systems. In *53rd IEEE conference on decision and control* (pp. 2802–2809).

Paulson, J. A., Streif, S., Findeisen, R., Braatz, R. D., & Mesbah, A. (2018). Fast stochastic model predictive control of end-to-end continuous pharmaceutical manufacturing. *vol. 41*, In *Computer aided chemical engineering* (pp. 353–378). Elsevier.

Petzke, F., Mesbah, A., & Streif, S. (2020). PoCET: A polynomial chaos expansion toolbox for Matlab. *IFAC-PapersOnLine*, *53*(2), 7256–7261.

Piprek, P., Gros, S., & Holzapfel, F. (2019a). A distributed robust optimal control framework based on polynomial chaos. In *CEAS EuroGNC conference on guidance, navigation and control* (pp. 1–20).

Piprek, P., Gros, S., & Holzapfel, F. (2019b). Rare event chance-constrained optimal control using polynomial chaos and subset simulation. *Processes*, *7*(4), 185.

Qin, S. J., & Badgwell, T. A. (2003). A survey of industrial model predictive control technology. *Control Engineering Practice*, *11*(7), 733–764.

Rahman, S. (2018). A polynomial chaos expansion in dependent random variables. *Journal of Mathematical Analysis and Applications*, *464*(1), 749–775.

Rawlings, J. B., Mayne, D. Q., & Diehl, M. (2017). *Model predictive control: Theory, computation, and design*. Santa Barbara, CA: Nob Hill Publishing.

Reizman, B. J., & Jensen, K. F. (2012). An automated continuous-flow platform for the estimation of multistep reaction kinetics. *Organic Process Research & Development*, *16*(11), 1770–1782.

Schmüdgen, K. (2017). The moment problem. *Graduate texts in mathematics*: *vol. 277*, Cham, Switzerland: Springer.

Shen, D. E., & Braatz, R. D. (2016). Polynomial chaos-based robust design of systems with probabilistic uncertainties. *AIChE Journal*, *62*, 3310—-3318.

Szegő, G. (1975). Orthogonal polynomials, *American mathematical society colloquium publications*, (4th ed.). Providence, RI: American Mathematical Society.

The MathWorks Inc. (2023). *MATLAB version: 23.2 (R2023b)*. Natick, MA: The MathWorks Inc., https://www.mathworks.com.

Tian, H., Prakash, J., Zavala, V. M., Olson, J. A., & Gopaluni, R. B. (2020). A tractable approximation for stochastic MPC and application to mechanical pulping processes. *Computers & Chemical Engineering*, *141*, Article 106977.

Trefethen, L. N. (2019). *Approximation theory and approximation practice, extended edition*. Philadelphia, PA: SIAM.

Van Hessem, D., & Bosgra, O. (2006). Stochastic closed-loop model predictive control of continuous nonlinear chemical processes. *Journal of Process Control*, *16*(3), 225–241.

von Andrian, M., & Braatz, R. D. (2019). Offset-free input-output formulations of stochastic model predictive control based on polynomial chaos theory. In *American control conference* (pp. 360–365).

von Andrian, M., & Braatz, R. D. (2020). Stochastic dynamic optimization and model predictive control based on polynomial chaos theory and symbolic arithmetic. In *American control conference* (pp. 3399–3404).

von Andrian-Werburg, M. F. (2024). *MPC quadratic dynamic matrix controler with soft constraints*. Natick, MA: The MathWorks Inc., https://www.mathworks.com/matlabcentral/fileexchange/73301-mpc-quadratic-dynamic-matrix-controler-with-soft-constraints.

Xiu, D., & Karniadakis, G. E. (2002). The Wiener-Askey polynomial chaos for stochastic differential equations. *SIAM Journal on Scientific Computing*, *24*(2), 619–644.

Zafiriou, E. (1990). Robust model predictive control of processes with hard constraints. *Computers & Chemical Engineering*, *14*(4–5), 359–371.

Zelen, M., & Severo, N. C. (1972). Probability functions. In M. Abramowitz, & I. A. Stegun (Eds.), *Handbook of mathematical functions with formulas, graphs, and mathematical tables* (10th ed.). (pp. 927–964). Washington, DC: United States Government Printing Office.

Zhou, K., & Doyle, J. C. (1998). *vol. 104*, *Essentials of robust control*. Upper Saddle River, NJ: Prentice Hall.

Zimmerman, R. D., Murillo-Sánchez, C. E., & Thomas, R. J. (2010). MATPOWER: Steady-state operations, planning, and analysis tools for power systems research and education. *IEEE Transactions on Power Systems*, *26*(1), 12–19.